



The impact of semi-open street roofs on urban pollutant exposure and pedestrian-level thermal comfort in 2-D street canyons

Huiru Zhong^a, Jiaxi Feng^a, Cho Kwong Charlie Lam^a, Jian Hang^{a,b,*}, Jiajia Hua^c, Zhongli Gu^d

^a School of Atmospheric Sciences, Sun Yat-sen University, Southern Marine Science and Engineering Guangdong Laboratory (Zhuhai), Zhuhai, PR China

^b Key Laboratory of Tropical Atmosphere-Ocean System (Sun Yat-sen University), Ministry of Education, Zhuhai, 519000, PR China

^c China Meteorological Administration Xiong'an Atmospheric Boundary Layer Key Laboratory, Xiong'an, PR China

^d Guangdong Fans-tech Agro Co., Ltd, PR China



ARTICLE INFO

Keywords:

Computational fluid dynamics simulation (CFD)
Outdoor thermal comfort
Pollutant exposure
Two-dimensional (2-D) street canyon
Urban microclimate
Semi-open street roofs (SOSRs)

ABSTRACT

Semi-open street roofs (SOSRs) have been confirmed to provide solar shading for pedestrians, usually improving outdoor thermal comfort but weakening urban ventilation in three-dimensional (3-D) urban districts. However, these positive and negative impacts have rarely been quantified together. Particularly, their impacts in two-dimensional (2-D) street canyons have not been investigated.

Accordingly, by conducting computational fluid dynamic (CFD) simulations coupling turbulence and radiation processes, this study investigates the integrated influences of SOSRs on both ventilation/pollutant exposure risks and pedestrian-level outdoor thermal comfort in 2-D full-scale street canyons (aspect ratios $AR = H/W = 1, 3, 5$; $W = 24$ m). Isothermal and non-isothermal cases with three solar angles (LST0900, LST1200, LST1500) are considered. The pedestrian-level maximum normalized velocity (V_{pedmax}/V_{inlet}) and physiological equivalent temperature (PET) are analyzed for ventilation and thermal comfort assessment.

SOSRs have an overall negative impact on present 2-D streets. Without SOSRs, only one main clockwise vortex exists when $H/W = 1$ and $H/W = 3$. Compared to the isothermal cases, LST0900 and LST1200 always strengthen this main vortex, while LST1500 weakens it slightly. The SOSRs may produce some secondary near-ground clockwise and counter-clockwise vortexes, which significantly reduce V_{pedmax}/V_{inlet} , i.e. from 0.33–0.44 to below 0.07 when $H/W = 1$ and 0.063–0.13 to 0.049 when $H/W = 3$. They also increase pedestrian-level PET by 0.9–10.4 °C ($H/W = 1$) and 0.1–4 °C ($H/W = 3$). When $H/W = 5$, two main vortexes appear in the isothermal case inducing much smaller V_{pedmax}/V_{inlet} of 0.004 and solar radiation significantly raises the V_{ped}/V_{inlet} to 3–25 times without SOSRs. The impacts of SOSRs are not as significant as those at $H/W = 1$ and 3. Overall, the SOSRs impact should be assessed before their application, especially in 2-D streets.

1. Introduction

Due to rapid urbanization, urban heat islands and air pollution have gained increased attention for their negative impacts on public health and outdoor thermal comfort during hot summer. Heating effects in urban areas result in higher air temperatures than in surrounding rural areas. For example, Chow et al. [1] reported that the maximum urban heat island intensity of 7 °C in Singapore. Uncomfortably high temperatures affect human health [2], likely increasing mortality and morbidity caused by air pollution [3]. Traffic emissions are major sources of urban air pollutants, including particulate matter (PM_{2.5}), carbon monoxide (CO), benzene, and nitric oxide. Exposure to high

pollutant concentrations is one of the major factors leading to health problems [4].

The aspect ratio (building height/street width, $AR = H/W$) is the first key factor influencing the amount of both incoming and outgoing radiation and the ventilation airflow in the street canyons [5]. Increasing the aspect ratio may reduce the sky view factor (SVF), subsequently decreasing the net outgoing long-wave radiation and the captured short-wave radiation, as well as street ventilation capacity. Past studies have proposed various mitigation strategies to alleviate the urban heat island intensity and improve outdoor thermal comfort [6–8], such as urban vegetation, water bodies, and adopting reflective materials on urban surfaces. As depicted in Fig. 1a, some urban designers suggest adopting artificial shading devices (i.e. semi-open street roofs, SOSRs) to

* Corresponding author. School of Atmospheric Sciences, Sun Yat-sen University, Southern Marine Science and Engineering Guangdong Laboratory (Zhuhai), Zhuhai, PR China.

E-mail address: hangj3@mail.sysu.edu.cn (J. Hang).

Nomenclature

$AR(H/W)$	aspect ratio
B	building width along stream-wise direction [m]
C_{co}	pollutant CO concentration [mg/m^3]
C_{ped}	pedestrian-level pollutant concentration [mg/m^3]
H	building height [m]
IF	population intake fraction [ppm, part per million]
L	building length along span-wise direction [m]
LST	local solar time
P_IF	personal intake fraction, the average IF for each person [ppm]
$\langle P_IF \rangle_{lee}$	the average personal intake fraction for the leeward side [ppm]
$\langle P_IF \rangle_{wind}$	the average personal intake fraction for the windward side [ppm]
$\langle P_IF \rangle$	the average personal intake fraction for two sides of the

PET	canyon [ppm]
Re	physiological equivalent temperature [$^\circ\text{C}$]
SVF	Reynolds number
T_{air}	sky view factor
T_{ref}	air temperature [$^\circ\text{C}$]
$\Delta T(T_{air}, T_{ref})$	background temperature [$^\circ\text{C}$] (32°C in this study)
ΔT_{ped}	relative air temperature compared with T_{ref} [$^\circ\text{C}$]
V	pedestrian-level relative air temperature [$^\circ\text{C}$]
V_{inlet}	velocity magnitude [m/s]
V/V_{inlet}	reference wind velocity [m/s]
V_{ped}/V_{inlet}	normalized velocity
V_{pedmax}/V_{inlet}	pedestrian-level normalized velocity
W	maximum pedestrian-level normalized velocity
W_s	street width [m]
x_i	CO source width [m]
	spatial coordinates ($i = 1, 2, 3$) in stream-wise (x), span-wise (y) and vertical directions (z) [m]

reduce the local exposure of direct solar radiation (positive impact) [9–14]. However, semi-open street roofs usually reduce urban wind speed, weaken ventilation capacity, and increase pollutant exposure (negative impact) [10]. Most previous studies emphasized such positive [9,13,15–17] and negative [18,19] impacts of the semi-open roofs separately in three-dimensional (3-D) urban environments. Hang et al. [18] verified that SOSRs weaken 3-D urban airflows and reduce urban ventilation. Some experimental and numerical investigations have verified that SOSRs or solar shading devices might provide solar shading and improve outdoor thermal comfort for pedestrians in 3-D urban environments [9,13,15]. They found that positive impacts of improving pedestrian-level thermal comfort are obvious in 3-D urban districts because the semi-open street roofs only reduce urban velocity slightly

but provide effective solar shading.

However, the impacts of SOSRs or solar shading devices on both pedestrian-level outdoor thermal comfort and ventilation/pollutant exposure risks in 2-D street canyons have not been widely studied. Paolini et al. [11] found that SOSRs may improve pedestrian-level thermal comfort in a wide street canyon with a low aspect ratio ($H/W = 0.18$). But some realistic urban districts consist of street canyons with tall buildings (i.e. $H/W = 1, 3, 5$) aligned at both sides (e.g. in Hong Kong, Manhattan or New York). Such street canyons can be simplified as two-dimensional (2-D) models when the approaching wind is perpendicular to the street axis, which attains the worst ventilation situation. The innovation of this paper is to quantify the influence of SOSRs on outdoor thermal comfort and urban ventilation/pollutant exposure in

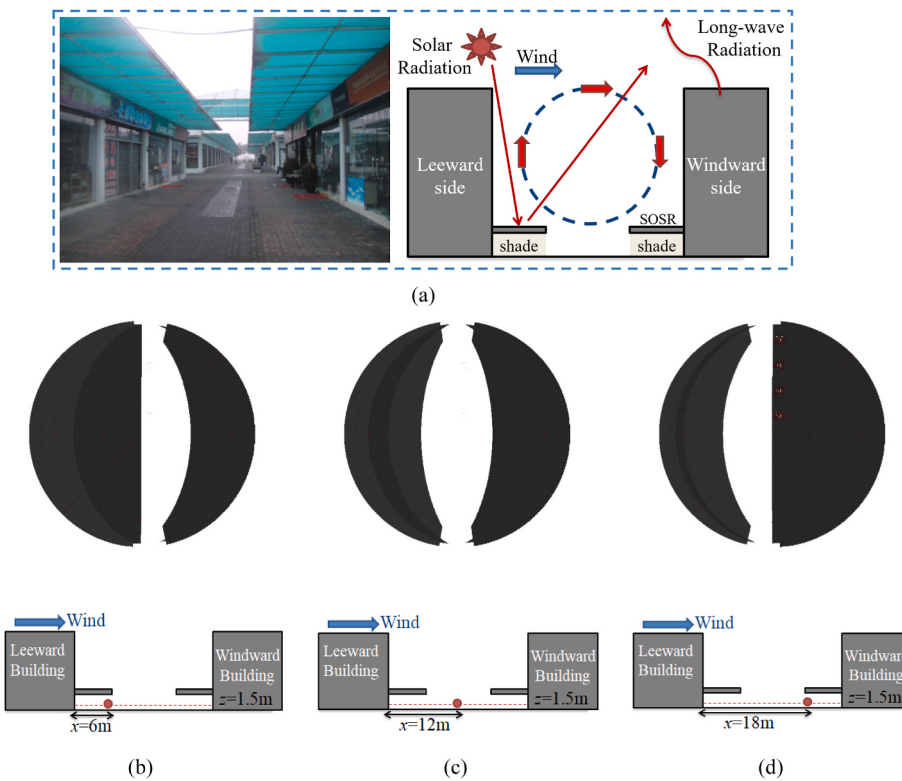


Fig. 1. (a) Configuration of semi-open street roofs in street canyons; Fish-eye images at pedestrian level ($z = 1.5$ m) when $H/W = 1$ ($W = 24$ m), obtained from SkyHelios: (b) $x = 6$ m, (c) $x = 12$ m, (d) $x = 18$ m.

2-D typical (e.g. $H/W = 1$), deep (e.g. $H/W = 3$) and extremely deep (e.g. $H/W = 5$) street canyons. To the best of our knowledge, this combined effect of SOSRs has not been investigated so far, especially rare for 2-D streets.

The 2-D street canyon model is a simplified urban geometry characterized by an infinitely long street (e.g. street length $L > 8H$) and the approaching wind direction perpendicular to the street axis. This model represents the worst ventilation scenario, attaining only ventilation through the urban canopy roof without turbulent exchange at the lateral boundaries. Despite its simplicity, the idealized 2-D urban street canyon models represent a form in real cities that has been widely investigated and is still being employed and examined in the literature [5,20–27].

Besides the thermal environment, air quality is a critical societal issue resulting in health problems. In particular, the integrated effects of SOSRs and street layouts on pollutant dispersion and pollutant exposure in 2-D street canyons are still unclear and require further studies. Numerous investigations have explored airflows and pollutant dispersion in urban street canyons without SOSRs, such as the impacts of building setbacks [28] and tree plantings [29]. Given that people spend 90% of their time indoors on average [21], pollutants exposure in near-road buildings requires more special concern. Some literature has adopted personal intake fraction (P_{IF}) to evaluate the exposure to pollutants [23,27,29–31], which indicates the fraction of total traffic pollutant inhaled by each person on average.

Few studies have simultaneously investigated the integrated impacts of urban buildings and SOSRs on the thermal environment, pedestrian-level thermal comfort, pollutant dispersion and their exposure risks in 2-D street canyons. To fill the current gap in the literature, this study aims to examine the integrated effects of street layouts and SOSRs on pedestrian-level thermal comfort, ventilation and pollutant exposure in idealized street canyons, using the CFD software ANSYS Fluent. This study addresses the impacts of SOSRs with the following research questions.

- (1) How do SOSRs and building configurations influence the wind velocity, air temperature and pedestrian-level thermal comfort in 2-D full-scale typical ($H/W = 1$), deep ($H/W = 3$) and extremely deep ($H/W = 5$) street canyons?
- (2) How do SOSRs and building layouts affect pollutant concentration in pedestrian regions and pollutants exposure in near-road buildings?

Outdoor thermal comfort is assessed by physiologically equivalent temperature (PET), a thermal comfort index calculated by the Rayman model [32]. Pollutant exposure is evaluated by personal intake fraction (P_{IF}). This paper is organized as follows. In Section 2, the indexes employed are presented (i.e., personal intake fraction and physiological equivalent temperature). Section 3 discusses the CFD methodology, including the description of cases, boundary conditions, and numerical method. Section 4 provides CFD validation. Section 5 discusses the impacts of aspect ratio and semi-open street roofs on flow and air temperature, pollutant distribution, pollutant exposure and pedestrian-level thermal comfort. Finally, section 6 shows the conclusions and study implication.

2. Indexes for thermal comfort and pollutant exposure

2.1. Thermal comfort index

To improve the prediction accuracy of thermal comfort, various thermo-physiological models have been established [33]. One of the most popular thermal indexes is Physiological Equivalent Temperature (PET), based on the Munich Energy-balance Model for Individuals (MEMI). PET can be calculated by the Rayman model, including air temperature, wind velocity, the time of day, cloud coverage and sky view factor (SVF) as the input [28,34]. In this study, the wind velocity

and air temperature values are from CFD validations. SVF can be obtained from fisheye images at 1.5 m above ground. Here, we use the SkyHelios model to generate the virtual fish-eye images (Fig. 1b–d) for each observation point by inputting a raster input file at a resolution of $0.5 \text{ m} \times 0.5 \text{ m}$ [34].

Due to the differences in the wind velocity and air temperature on different sidewalks, 11 observation points were chosen to better characterize the thermal comfort at pedestrian-level height ($z = 1.5 \text{ m}$). The observation points are arranged 2 m away from the building's wall and the interval between each observation point is 2 m. As shown in Table 1, the outcomes were analyzed according to the thermal sensation classifications for Physiological Equivalent Temperature (PET) in Singapore [35] since Singapore has high temperatures and high humidity all year round.

2.2. Pollutant exposure assessment

Population intake fraction (IF) was introduced to quantify traffic pollutant exposure in former studies [21,23,27,29,30], representing the proportion of air pollutants inhaled by the whole exposed population. If $IF = 1 \text{ ppm}$ (part per million), it indicates that 1 mg of pollutant is inhaled by the exposed population from 1 kg of pollutant emission. Some literature has estimated the IF in the city. For example, Luo et al. [4] reported that vehicular CO IF s are 270 ppm in Hong Kong.

For a specific pollutant, IF is defined as Eq. (1).

$$IF = \sum_p^N \sum_q^M P_p \times Br_{p,q} \times \Delta t_{p,q} \times Ce_q / m \quad (1)$$

where m (kg) is the total pollutant emission by vehicles over the period considered. N and M are the amount of population groups and micro-environments, respectively. As depicted in Table 2, the whole population is divided into three age groups ($N = 3$) based on the population census data [4], namely Children ($p = 1$), adults ($p = 2$) and elders ($p = 3$). Moreover, we consider four micro-environments ($M = 4$) according to the former literature [36,37], i.e. indoors at home ($q = 1$), other indoor locations ($q = 2$), near vehicles ($q = 3$) and other outdoor locations away from vehicles ($q = 4$). $Br_{p,q}$ represents the average volumetric breathing rate for individuals. P_p is the exposed population amount in the p^{th} age group. Ce_q (kg/m^3) stands for the time-averaged pollutant concentration caused by traffic emissions in the q^{th} micro-environment. $\Delta t_{p,q}$ stands for the time the p^{th} age group spends in the q^{th} micro-environment.

Furthermore, to eliminate the impact of exposed population size and density, this study adopts person intake fraction (P_{IF}) to characterize traffic pollutant exposure. P_{IF} is the average IF for each person of a population equally distributed in all buildings on both sides of the street canyon [21,23,27,29,30]. P_{IF} is given by Eq. (2).

$$P_{IF} = IF / \sum_p^N P_p \quad (2)$$

Table 1

Thermal sensation classifications for Physiological Equivalent Temperature (PET) in Singapore (adapted from Yang et al. [35]).

PET($^{\circ}\text{C}$)	Thermal sensation
Not applicable	Very cold
Not applicable	Cold
Not applicable	Cool
20–24	Slightly cool
24–30	Neutral
30–34	Slightly warm
34–38	Warm
38–42	Hot
>42	Very hot

Table 2

(a) Time activity patterns in four microenvironments for adults, children and elders; (b) Time activity patterns with indoor at home ($q = 1$), breathing rate and population for each age group.

Age groups	$q = 1$	$q = 2$	$q = 3$	$q = 4$
Adults(18–60)	59.50%	28.70%	7.10%	4.70%
Children(<18)	61.70%	28.90%	5.50%	3.90%
Elders(>60)	71.60%	16.68%	3.20%	8.59%

Age groups	Time pattern (%)	Breathing rate(m^3/day)	Population (%)
Adults(18–60)	59.5%	13.8	63.3%
Children(<18)	61.7%	12.5	21.2%
Elders(>60)	71.6%	13.1	15.5%

This study assumes that the buildings are residential, so only pollutants in one micro-environment (i.e. $q = 1$, indoor at home) are considered [27,29,30]. C_{eq} ($q = 1$) stands for pollutant concentration indoors at home, regarded as the pollutant concentration on the building wall surface originating from the outdoor vehicular emissions. In this study, the average personal intake fraction on the leeward-wall, windward-wall and both two sides of the street canyon are defined as $\langle P_{IF} \rangle_{le}, \langle P_{IF} \rangle_{wind}$ and $\langle P_{IF} \rangle$.

3. CFD methodology

3.1. Description of case studies in numerical simulations and simulation setup

As shown in Fig. 2a, the full-scale two-dimensional (2-D) street

canyon models are composed of five uniform buildings. Both building width (B) and street width (W) are 24 m. Three street aspect ratios ($AR = H/W = 1, 3, 5$) are adopted (i.e., $H = 24$ m, 72 m, 120 m), these three aspect ratios are typical in previous literature [23,30,38,39]. According to the literature [39–41], flow regimes in 2-D street canyons can be categorized into four types in the isothermal case, i.e. the isolated roughness flow regime ($H/W < 0.3$), the wake interference flow regime ($0.3 < H/W < 0.7$), the skimming flow regime ($0.7 < H/W < 1.57$), and multi-vortex flow regime ($H/W > 1.57$). Based on wind-tunnel-scale street canyon models, the literature [39–41] reported that there is only one main vortex when $H/W = 1$, two counter-rotating vortices when $H/W = 2$ and three to five vertically-aligned vortices are formed when $H/W = 3$ and 5 ($H = 0.06$ m, $Re \sim 12,000$). However, for some full-scale street canyons ($H \sim 10$ –100 m), the literature has demonstrated different findings [27,30], i.e. only one clockwise vortex when $H/W = 3$ and two opposite vortices when $H/W = 5$ in the isothermal case. In general, to achieve Reynolds number independence in urban airflow, the value of Re should be much greater than 11,000. Full-scale models (e.g. $H = 24$ m, 72 m, 120 m; $W = 24$ m) generally fulfill this Re -independence requirement, whereas wind-tunnel-scale models sometimes cannot meet this requirement.

Fig. 2a displays an example of $W \times L \times H = 24$ m \times 12 m \times 72 m when $H/W = 3$ and displays the detailed descriptions of the target street. The third street is the target street and other street canyons in the upstream and downstream regions are set to simulate the roughness elements effect.

SOSRs are installed on both sides of the target street, with a height of 4 m and a width of 6 m. The geometry setting of the SOSRs in some literature can be found in Table 3. In this study, semi-open street roofs are installed on both sides of the target street. The semi-open street roofs have a height of 4 m and a width of 6 m, which falls within the range of

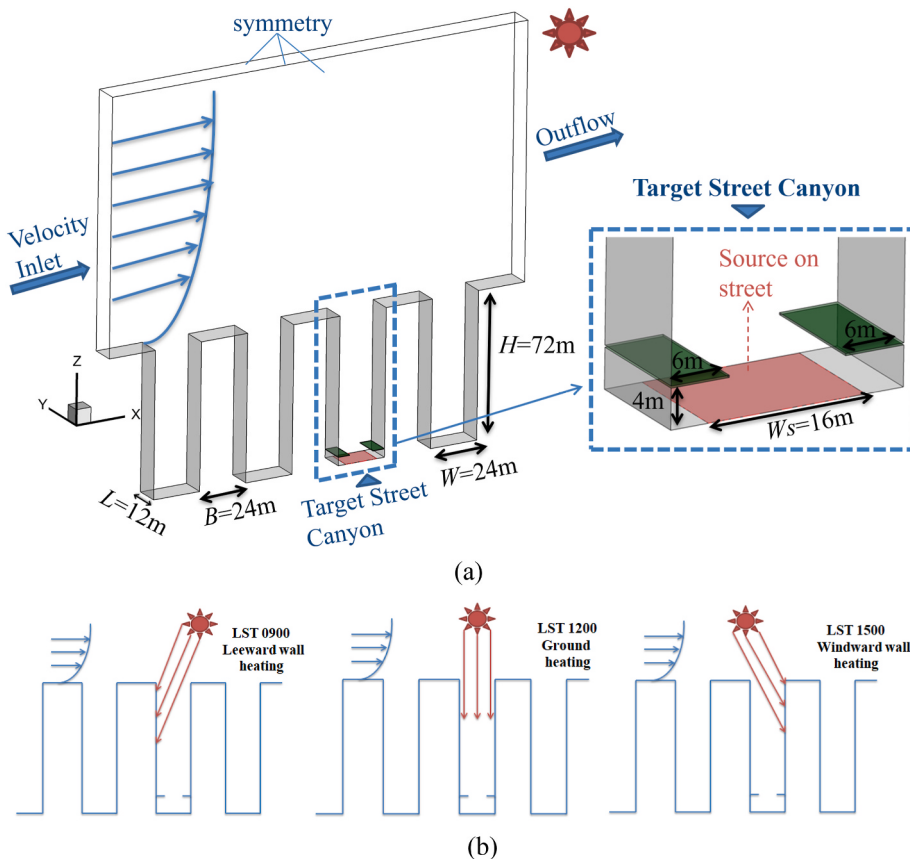


Fig. 2. (a) Computational domain and target street canyon as an example (e.g. $H/W = 3$, $W = 24$ m, $H = 72$ m), (b) Sketch of solar scenarios with solar angles at LST0900, LST1200 and LST1500.

Table 3

The geometry setting of the semi-open street roofs or solar shading devices in some literature.

	Street width (W)	Semi-open street roofs width	Semi-open street roofs heights
Hang et al., 2013	7 m	5.6–7 m	7–10.5 m
Paolini et al., 2014	55 m	35 m	10 m
Nasrollahi et al., 2020	18 m		4–8 m
Elnabawi et al., 2020	4 m	4 m	7 m
Lee et al., 2020	5.4 m	3.64 m	4.09 m
Lam et al., 2022		3–12 m	3–12 m

settings in the previous literature. As displayed in Fig. 2a, the street is half-open and half-closed, namely allowing a certain degree of ventilation capacity. The radiation and energy properties of semi-open street roofs and building surfaces are provided in Table 4, which are similar to standard concrete [42]. Apart from considering the impact of SOSRs and aspect ratios, to simulate a more real situation, the thermal boundary conditions of the ground, wall and atmosphere at a different local solar time (LST) are set by Solar Tracing Model. As depicted in Fig. 2b, this study investigates the situation at different solar angles, i.e. LST0900 (leeward side wall solar heating), LST1200 (ground solar heating) and LST1500 (windward side wall solar heating).

The longitude of the simulated geographical location is 113.14°E and the time zone is +8 GMT. To guarantee the two-dimensional properties of the street canyon, the latitude is fixed at 0° and the simulated date is set to the autumnal equinox (22nd September). This geographical coordinate represents typical tropical cities. Since we simulate a north-south street canyon, the solar angle vector has no component in y direction. The P-1 radiation model is selected, which has been adopted in a previous case study [27]. Direct solar radiation and diffuse solar radiation are solved by the solar calculator of ANSYS Fluent 15.0.

The left side of the computational domain is set as the inflow boundary, and the right side is set as the outflow boundary (Fig. 2a). To ensure the two-dimensional properties of the street canyon, the top and two lateral zones of the computational domain are set as symmetrical boundaries. Moreover, the approaching wind is perpendicular to the street axis. The selected inflow scheme is the atmospheric boundary layer (ABL) velocity inflow scheme in the full-scale street scale. Based on this scheme, the inlet wind speed (U_0), turbulent kinetic energy (k_{in}) and turbulent kinetic energy dissipation (ϵ_{in}) are given in the form of profile, as shown in Eqs. (3)–(5).

$$U_0(z) = U_{ref} \left(\frac{z - H}{z_{ref}} \right)^{\alpha} \quad (3)$$

$$k_{in}(z) = (U_{in}(z) \times I_{in})^2 \quad (4)$$

$$\epsilon_{in}(z) = \frac{C_{\mu}^{3/4} k_{in}^{3/2}}{\kappa z} \quad (5)$$

Table 4
Radiation and energy properties.

	Density (kg/m ³)	Specific heat (J/ kgK)	Thermal conductivity (W/mK)	Absorptivity	Emissivity
Surfaces/ Semi- open street roofs	1400	900	1.7	0.75	0.88
Street ground	1400	900	1.7	0.6	0.9

where the reference velocity (U_{ref}) is 3 m/s obtained from the reference height (z_{ref}) of 24 m above the building roof. In this study, we changed the “H” for each depth. $H = 24$ m, 72 m and 120 m are adopted in three street aspect ratios ($H/W = 1, 3, 5$). This setting is to ensure the velocity at the building roof surface (i.e. as $z = H$) is zero, satisfying the no-slip boundary condition. The power-law exponent α is set to 0.22. Turbulence intensity (I_{in}) is 0.1, Von Karman constant (κ) is 0.41, and empirical constant (C_{μ}) is 0.09.

The Reynolds number independence criterion, $Re > 11,000$ is widely applied to estimate the dynamic similarity in the simulation. It means when the Reynolds number is much greater than 11,000, the Reynolds independent condition is satisfied, and the turbulence is fully developed [43]. In other words, the flow pattern does not change significantly with the increase of Re . However, the widely adopted criterion $Re > 11,000$ is unsuitable for full-scale 2-D deep street canyons [44,45]. Yang et al. [44] reported that for deep street canyons ($H/W = 3$ and 5, $W = 24$ m) Reynolds independence can be achieved when Re exceeds the critical Re ($Re \sim 10^6, 10^7$ when $H/W = 3, 5$). In this study, the reference Reynolds number based on the reference building height ($H = 24$ m, $U_{ref} = 3$ m/s) is about 4×10^6 when $H/W = 1$, which is much larger than 11,000. For deep and extremely deep street canyons ($H/W = 3, 5$), Re is about 1.2×10^7 and 2×10^7 , which is larger than 10^6 and 10^7 respectively.

Sufficiently fine grids at the regions close to building surfaces and grounds are needed. Thus the minimum wall grid is set to 0.1 m. The total number of grids for all cases ranges from 0.8 to 5.0 million and Table 5 lists all test cases.

3.2. Numerical models

This study adopted the method of computational fluid dynamics (CFD). The previous studies reported that the large eddy simulations (LES) perform better than Reynolds-Averaged Navier-Stokes (RANS) approach in predicting turbulence [46,47]. However, LES takes more computing time and resources than RANS approaches. Moreover, LES has some challenges regarding implementing appropriate boundary conditions and advanced sub-grid scale models. Thus, considering RANS turbulence models can save more time and supply reasonable results for mean flows and the spatial average flow properties [46], much literature still adopts RANS turbulence models [23,27,29,30]. In various RANS models (e.g., various $k-\varepsilon$ and $k-\omega$ models), the standard $k-\varepsilon$ better predicts airflow velocity and pollutant dispersion in urban areas [18,19, 31]. Hence, the standard $k-\varepsilon$ model is adopted to simulate the urban airflow with the 2-D street canyons in this paper.

The governing equations of mass conservation, momentum, turbulent kinetic energy and its dissipation rate were listed in detail in previous literature [30]. They were discretized by the finite volume method (FVM) with a second-order upwind scheme to ensure the simulation accuracy. Moreover, this study uses the SIMPLE (Semi-Implicit Method for Pressure-Linked Equations) scheme to couple pressure and velocity. The under-relaxation factors of momentum term, pressure term, k term and ε term are 0.7, 0.3, 0.8 and 0.8, respectively. Furthermore, the

Table 5
Test cases investigated in this study.

Case name	H/W (W = 24 m)	Semi-open street roofs	Reference velocity	Sun positions
Case [1]	1			NULL LST0900
Case [3]	3	NO		
Case [5]	5		3 m/s	
Case[1, Semi]	1			LST1200
Case[3, Semi]	3	YES		LST1500
Case[5, Semi]	5			

convergence criterion of the equations was set to 1×10^{-6} .

3.3. Description of pollutant dispersion modeling

As depicted in Fig. 2a, the vehicular emission is set on the ground of the target street with a height of 0.2 m (z), span-wise width of 12 m (y) and stream-wise length (W_s) of 16 m (x). Carbon monoxide (CO) was selected as the traffic pollutant emission owing to its relatively inert chemical property [21,30]. Eq. (6) is the governing equation of time-averaged CO concentration C (kg/m^3).

$$\bar{u}_j \frac{\partial C}{\partial x_j} - \frac{\partial}{\partial x_j} \left[(D_m + D_t) \frac{\partial C}{\partial x_j} \right] = S \quad (6)$$

where, \bar{u}_j is the time-averaged velocity component of direction j . D_m represents the molecular of pollutant, and D_t represents the turbulent diffusivity of pollutant. Proof by the function $D_t = \frac{\nu_t}{S_{ct}}$ (ν_t represents the kinematic eddy viscosity and S_{ct} stands for the turbulent Schmidt number), D_t varies with S_{ct} and will affect pollutant dispersion. S is the realistic CO emission rate, and its value is $1.25 \times 10^{-6} \text{ kg/m}^3/\text{s}$ [21,29]. In this study, the CO emission rate and geometry size were the same in

all cases.

4. CFD validation

The numerical models are validated by wind tunnel experiments at the University of Gavle, Sweden [30]. As shown in Fig.A1, there are 25 rows of building models, and the dimension of the working section is 11 m \times 3 m \times 1.5 m (length \times width \times height). For wind-tunnel-scale street canyon models, the building height (H), building width (B) and street width (W) are 0.12 m, 0.05 m and 0.05 m respectively, resulting in a street aspect ratio of $H/W = 2.4$. Moreover, the span-wise length is 1.25 m larger than $8H$ to ensure the 2-D properties of the street canyon [40]. In wind tunnel experiments, the approaching air flow is perpendicular to the street axis with the reference wind speed $U_{ref} = 13 \text{ m/s}$.

The CFD simulation of the full-scale street canyon models ($H = 24 \text{ m}$, $W=B=10 \text{ m}$) for validation is investigated using ANSYS Fluent together with the standard $k-\epsilon$ turbulence model. The ratio of the full-scale street canyon model to wind-tunnel-scale models ($H = 12 \text{ cm}$) is 200:1. As displayed in Fig.A1, Laser Doppler Anemometer (LAD) System measures the mean wind speed and turbulence intensities along the street

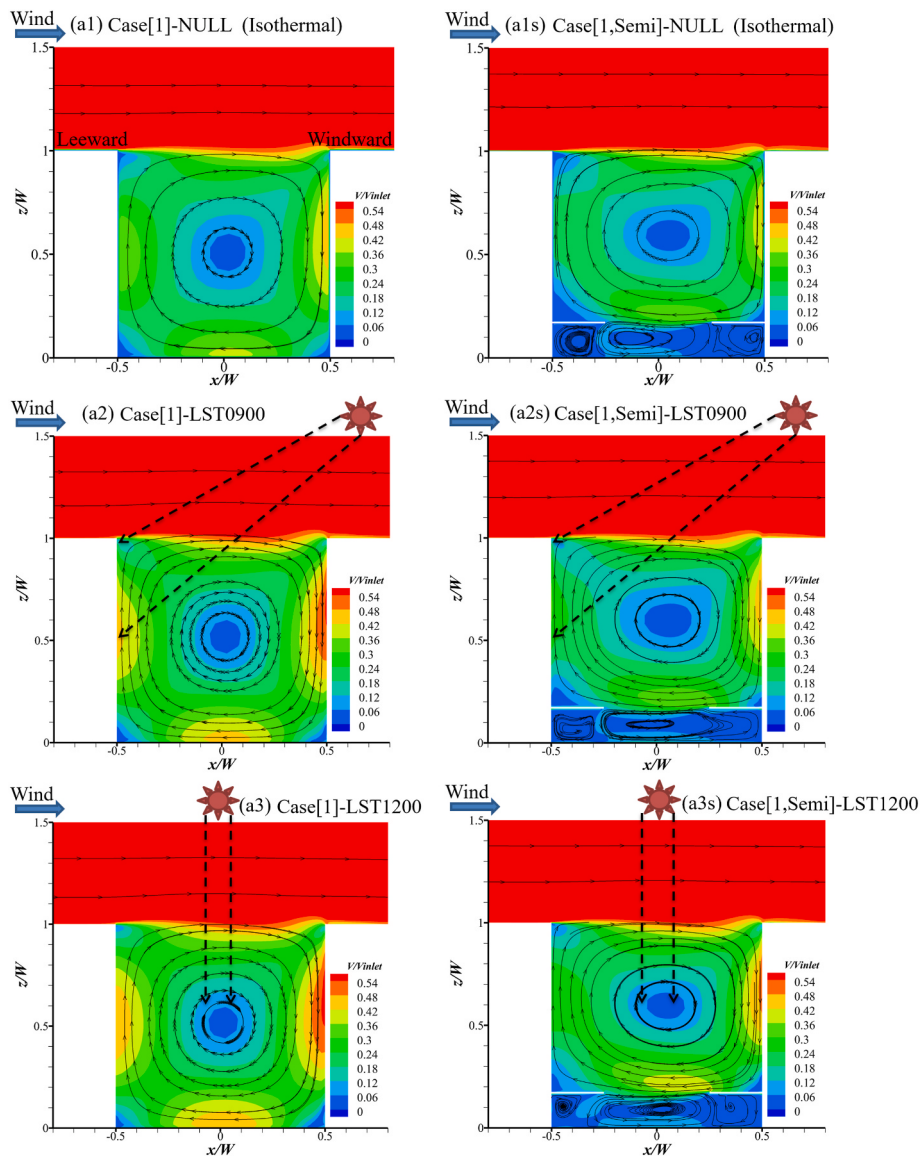


Fig. 3. In the x - z central plane for cases with/without semi-open street roofs when $H/W = 1$: (a) 2-D Streamlines and normalized velocity (V/V_{inlet}), (b)Horizontal profiles of V_{ped}/V_{inlets} (c) relative air temperature ($\Delta T = T_{air}-T_{ref}$), (d) Horizontal profiles of ΔT_{ped} .

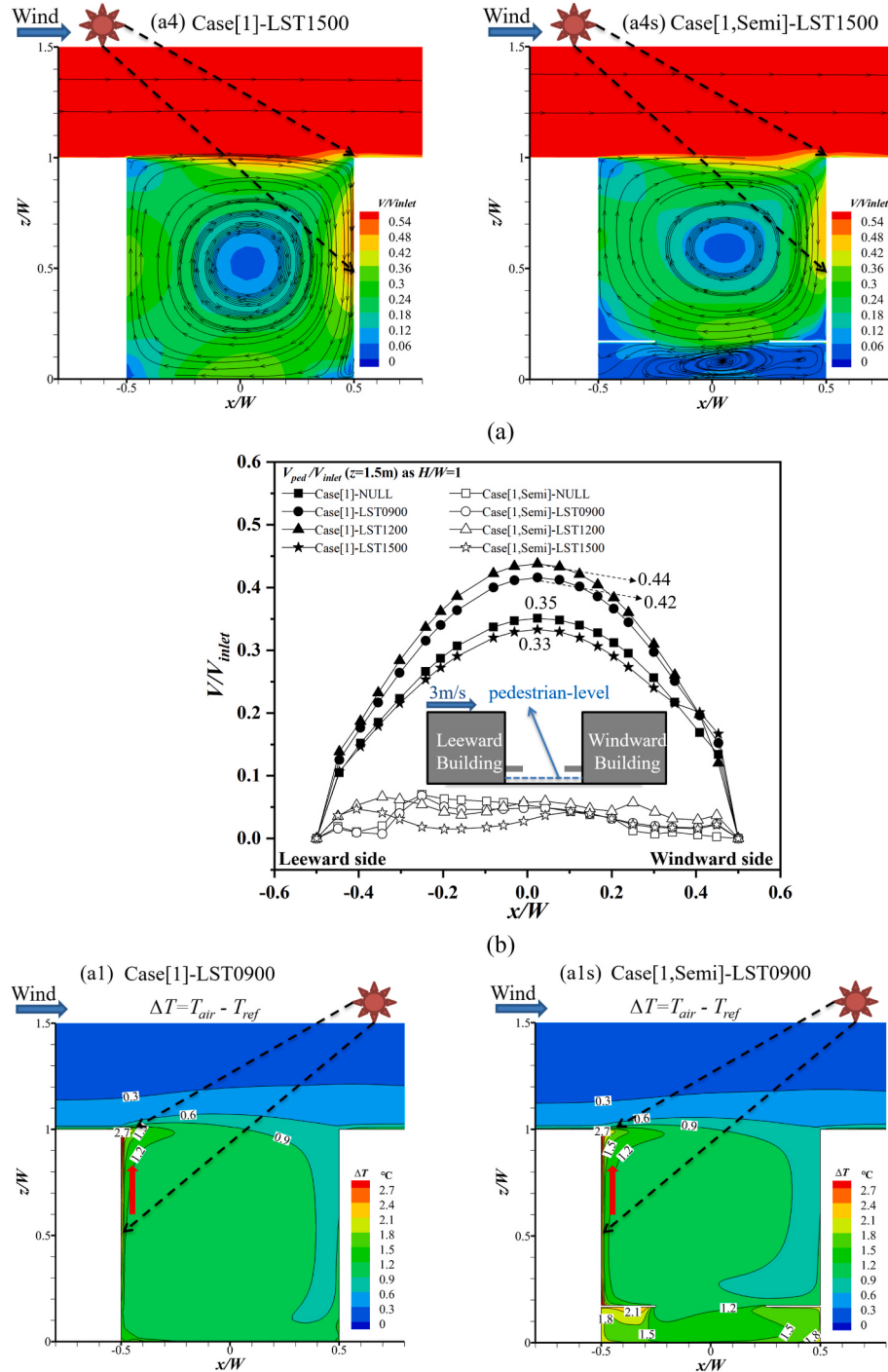


Fig. 3. (continued).

centerline of Line E and Line F (Fig.A1). In this study, the domain inlet boundary conditions are set on the basis of measurement results in wind tunnel experiments, including stream-wise velocity and turbulent kinetic energy at Line E.

Fig.A2 shows the CFD simulation results and wind tunnel data by the stream-wise velocity profiles at Line F. In general, the predicted wind profile coincides well with the wind tunnel data and the major vortex structure was formed in the street canyon when $H/W = 2.4$. In addition, the simulation results are relatively consistent with the wind tunnel data for the normalized turbulent kinetic energy.

5. Results and discussion

5.1. Impacts of aspect ratio and semi-open street roofs on air flow and air temperature

5.1.1. In typical street canyon ($H/W = 1$)

Fig. 3 shows the 2-D streamline, normalized velocity (V/V_{inlet}) and relative air temperature ($\Delta T = T_{air} - T_{ref}$) at the x - z central plane and along the line at the pedestrian level ($z = 1.5$ m) for typical street canyons ($H/W = 1$) with and without semi-open street roofs under isothermal and three solar scenarios. Here T_{ref} ($=32^{\circ}\text{C}$) is the background air temperature, and V_{inlet} ($=3$ m/s) is the background velocity of the domain inlet.

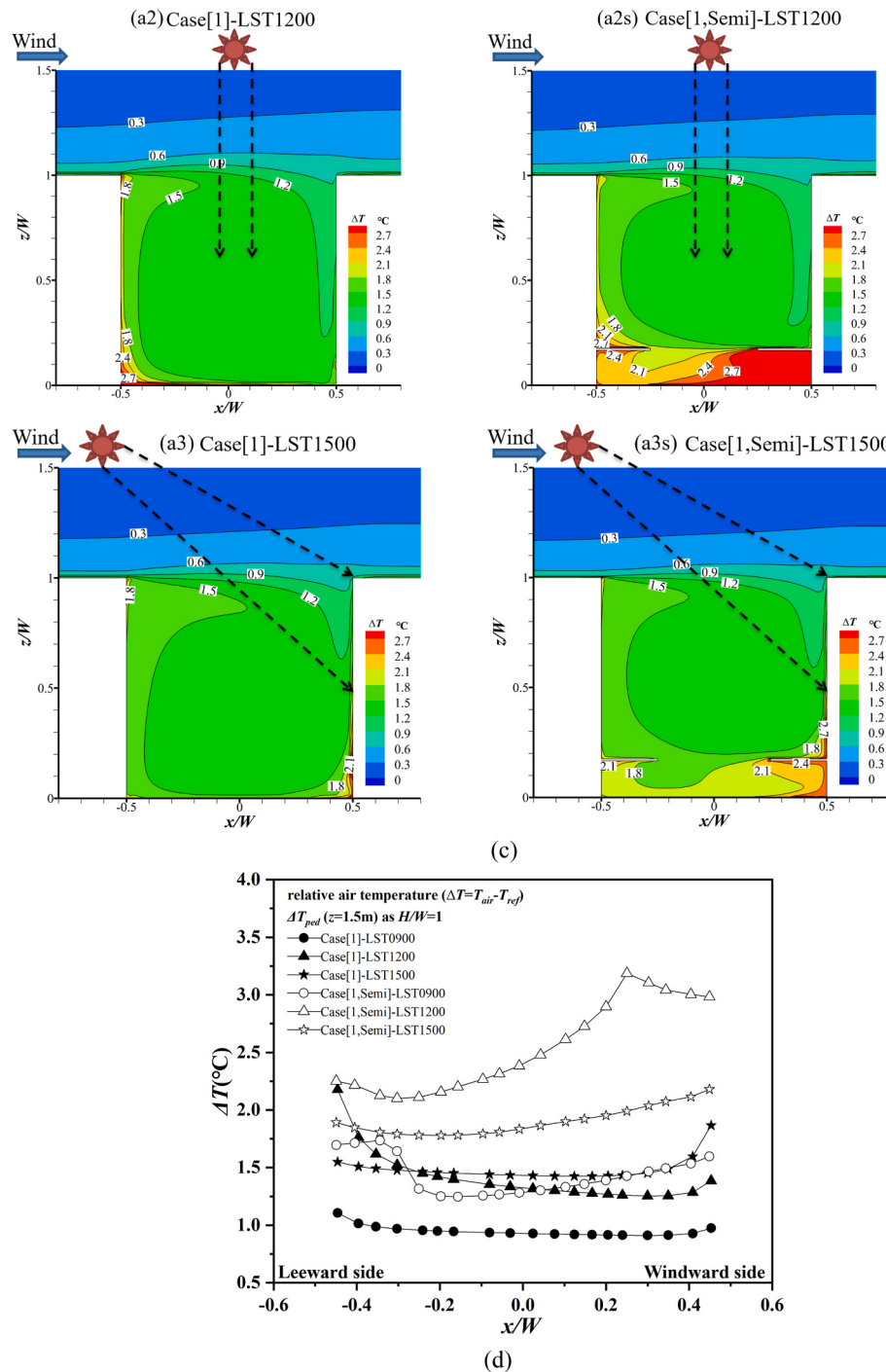


Fig. 3. (continued).

Without SOSRs (Fig. 3a), there is only one main clockwise vortex under different solar conditions. Due to the interaction of thermal buoyancy force and air flow, LST0900 (directly leeward heating) and LST1200 (directly ground heating) enhance this vortex flow structure while the circulation is weaker at LST1500 (directly windward wall heating). The above physical phenomena are the same as the findings reported by the literature of numerical simulations [27,48] and are consistent with those found by wind tunnel experiments [49]. Fig. 3b depicts the quantitative impacts. Without SOSRs, compared to the isothermal case ($V_{pedmax}/V_{inlet} \sim 0.35$), solar radiation significantly increases V_{ped}/V_{inlet} at LST0900 and LST1200 ($V_{pedmax}/V_{inlet} \sim 0.42$ and 0.44), but slightly decreases V_{ped}/V_{inlet} at LST1500 ($V_{pedmax}/V_{inlet} \sim 0.33$),

which are consistent with the physical phenomena in Fig. 3a.

In addition, when SOSRs are constructed (Fig. 3a), an upper main clockwise vortex appears, and some much weaker clockwise and counter-clockwise vortexes below the SOSRs height occur under all solar radiation conditions. As a result, Fig. 3b displays that, V_{ped}/V_{inlet} becomes less than 0.07 in all solar conditions, much less than those without SOSRs, namely 5–30 times (LST0900), 4–10 times (LST1200), 3–19 times (LST1500) and 4–35 times (isothermal case) lower than those without SOSRs.

Fig. 3c displays relative air temperature ($\Delta T = T_{air} - T_{ref}$) at the central $x-z$ plane when $H/W = 1$. SOSRs hardly influence ΔT below the SOSRs height by about 0.2–1.5 °C. Especially at LST1200, the air temperature

at the pedestrian level becomes much higher due to the SOSRs. As displayed in Fig. 3d, SOSRs significantly raise the horizontal profiles of pedestrian-level (ΔT_{ped}). Without SOSRs, ΔT_{ped} ranges from 1 to 2.5 °C, and if SOSRs are installed, ΔT_{ped} (1.3–3 °C) is higher in most regions. More specifically, ΔT_{ped} with SOSRs is 1.3–1.8 times (LST0900), 1.3–2.5 times (LST1200) and 1.2–1.4times (LST1500) higher than that without it. In other words, the maximum increase of ΔT_{ped} is 76% at LST0900, 152% at LST1200 and 40% at LST1500. In addition, at LST1200, the leeward-side ΔT_{ped} is greater than that at the windward-side without SOSRs while the situation is opposite with SOSRs (Fig. 3d). The reason is mainly related to the corresponding clockwise or counter-clockwise vortex in the street canyon. Without SOSRs, the clockwise vortex accumulates heat at the bottom of the leeward side (Fig. 3a, c). However, when SOSRs are installed, the newly formed weaker vortices below the SOSRs cause heat to accumulate at the bottom of the windward side at LST1200 (Fig. 3a, c).

5.1.2. In deep street canyon ($H/W = 3$)

For deep street canyons ($H/W = 3$) with and without SOSRs under four solar radiation conditions, Fig. 4 displays 2-D streamline,

normalized velocity (V/V_{inlet}) and relative air temperature ($\Delta T = T_{air} - T_{ref}$) at $x-z$ central plane and their horizontal profiles along the line at the pedestrian-level ($z = 1.5$ m).

As shown in Fig. 4a, without SOSRs, there is still one clockwise main vortex formed at the isothermal case ($V_{pedmax}/V_{inlet} \sim 0.066$, see Fig. 4b), LST0900 ($V_{pedmax}/V_{inlet} \sim 0.074$) and LST1200 ($V_{pedmax}/V_{inlet} \sim 0.13$). Their values are weaker than those when $H/W = 1$ ($V_{pedmax}/V_{inlet} \sim 0.35, 0.42, 0.44$ at the isothermal case, LST0900 and LST1200). Moreover, the main vortex at LST0900 and LST1200 is stronger than that at the isothermal case. However, at LST1500 ($V_{pedmax}/V_{inlet} \sim 0.063$), a clockwise vortex appears in the upper part and a much weaker counter-clockwise vortex in the lower part of the street canyon (Fig. 4a). This is mainly because at LST1500, solar radiation directly heats the windward wall. Therefore, the windward-side upward thermal buoyancy force hinders the clockwise downward flow, resulting in the destruction of the single vortex structure and the appearance of the counter-clockwise vortex [48]. When SOSRs are constructed, some small vortices are generated under the SOSRs height (Fig. 4a). To better quantify this impact, Fig. 4b displays that installing SOSRs decreases V_{ped}/V_{inlet} from 0.066–0.13 to below 0.049.

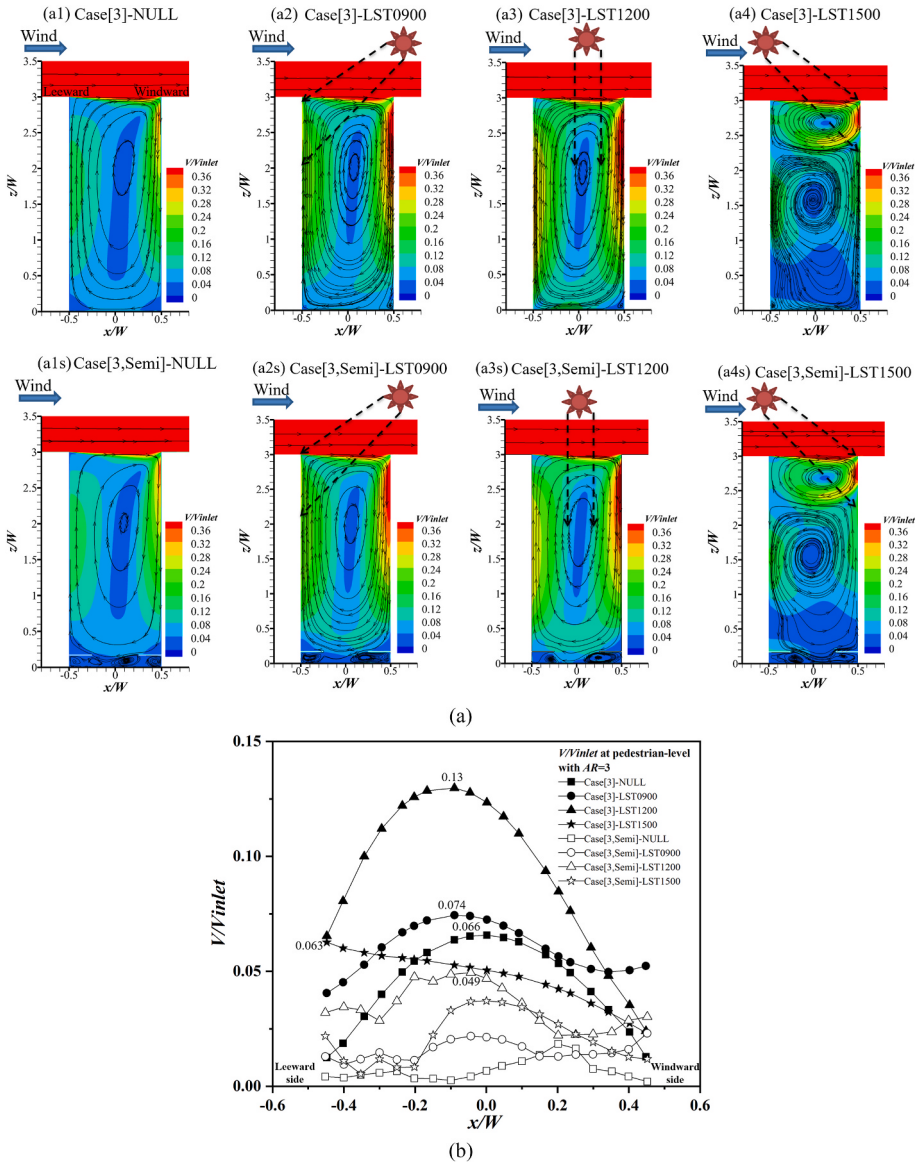


Fig. 4. In the $x-z$ central plane for cases with/without semi-open street roofs when $H/W = 3$: (a) 2-D Streamlines and normalized velocity (V/V_{inlet}), (b) Horizontal profiles of V_{ped}/V_{inlets} (c) relative air temperature ($\Delta T = T_{air} - T_{ref}$), (d) Horizontal profiles of ΔT_{ped} .

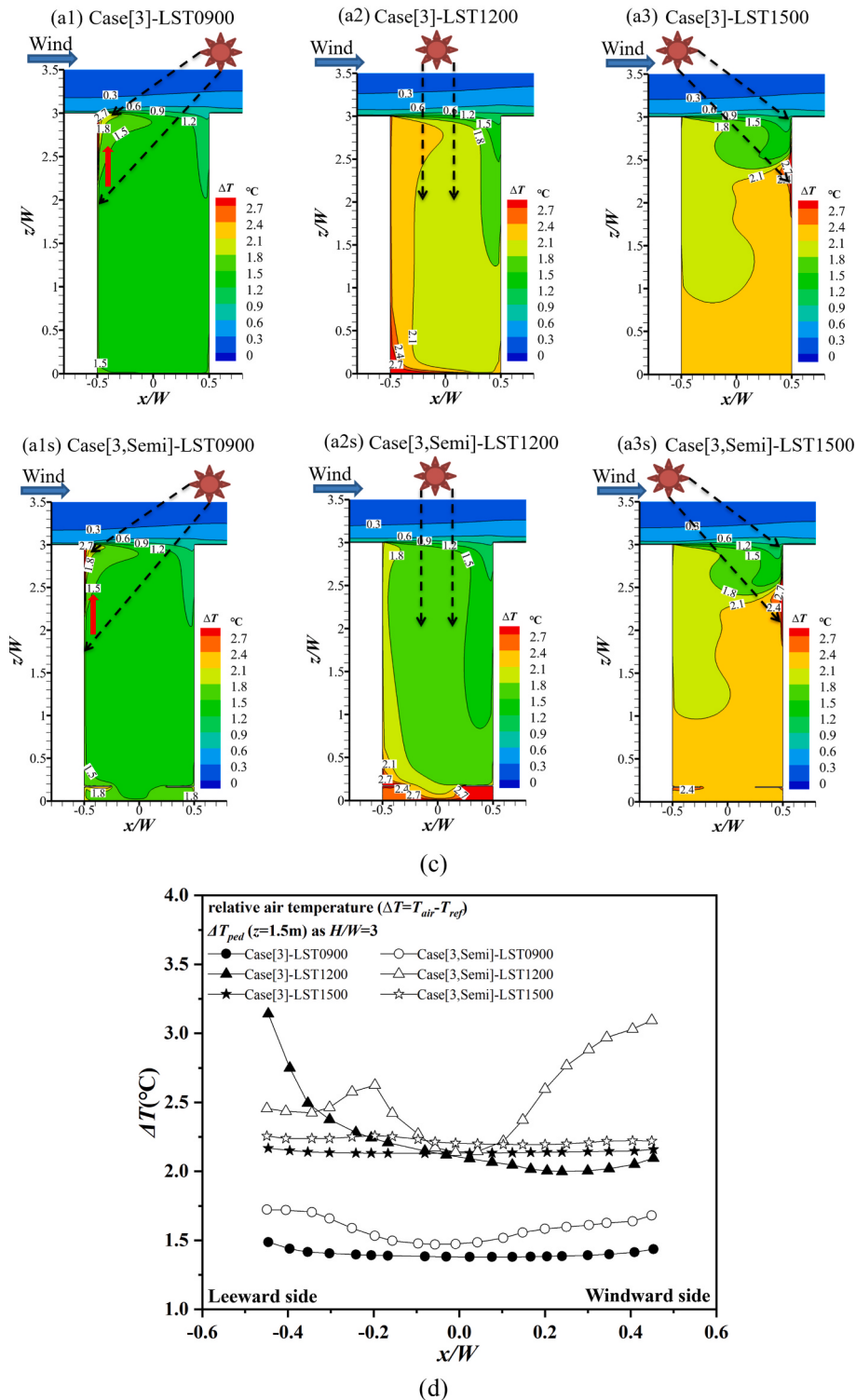


Fig. 4. (continued).

For the thermal environment in the deep street canyon ($H/W = 3$, see Fig. 4c), when SOSRs are installed, the relative air temperature (ΔT) in the street canyon changes slightly under the solar angles of LST0900 and LST1500. Because the tall building makes a major contribution to shading. The SOSRs contribute only a little. However, ΔT below the SOSRs height increases significantly under the solar angle of LST1200. Fig. 4d further quantifies the impact of SOSRs on ΔT_{ped} . Without SOSRs, ΔT_{ped} is about 1.4°C at LST0900, $2\text{--}3^{\circ}\text{C}$ at LST1200 and 2.1°C at LST1500, which is higher than those when $H/W = 1$ ($\Delta T_{ped} \sim 0.95^{\circ}\text{C}$,

$1.3\text{--}2.2^{\circ}\text{C}$ and 1.5°C at LST0900, LST1200 and LST1500 respectively, see Fig. 3d). It indicates that ΔT_{ped} for deep street canyons ($H/W = 3$) is about $0.5\text{--}0.8^{\circ}\text{C}$ higher than that in typical street canyons ($H/W = 1$). Furthermore, compared with the case without SOSRs ($H/W = 3$), the setup of SOSRs raises ΔT_{ped} slightly, namely 1.2 times (LST0900), 1.5 times (LST1200) and 1.1 times (LST1500) higher than that without SOSRs. Besides, as depicted in Fig. 4d, under the solar angle of LST1200, ΔT_{ped} is higher on the leeward side without the SOSRs while ΔT is higher on the windward side after installing the SOSRs.

5.1.3. In extremely deep street canyon ($H/W = 5$)

For extremely deep street canyons ($H/W = 5$), Fig. 5 displays 2-D streamline, normalized velocity and relative air temperature at the x - z central plane and their horizontal profiles at the pedestrian level with and without SOSRs. As displayed in Fig. 5a, there are a clockwise vortex and a counter-clockwise vortex without SOSRs at the isothermal conditions. At LST0900 and LST1200, thermal buoyancy force destroys this two-main-vortex structure, producing a major clockwise vortex in the entire street canyon. Moreover, three vortices are observed under the solar angle of LST1500 (Fig. 5a). When SOSRs are constructed, there is only one main clockwise vortex under isothermal conditions, LST0900 and LST1200. However, under the solar angle of LST1500, three main vortices are still observed and some small vortices are formed under the SOSRs height. Fig. 5b depicts the horizontal profiles of pedestrian-level ($z = 1.5$ m) V/V_{inlet} to better quantify the impact of SOSRs. Without SOSRs (Fig. 5b), compared with the isothermal case ($V_{pedmax}/V_{inlet} \sim 0.004$), the buoyancy force induced by solar radiation raises the V_{ped}/V_{inlet} to 3–25 times ($V_{pedmax}/V_{inlet} \sim 0.025$, 0.102 and 0.011 at

LST0900, LST1200 and LST1500 respectively). Besides, compared with the typical street canyons (i.e. $V_{pedmax}/V_{inlet} \sim 0.35$ and 0.44 at the isothermal case and LST1200 when $H/W = 1$, see Fig. 3b) and deep street canyons (i.e. $V_{pedmax}/V_{inlet} \sim 0.066$ and 0.13 at the isothermal case and LST1200 when $H/W = 3$, Fig. 4b), the influence of solar radiation on V_{ped}/V_{inlet} is stronger when $H/W = 5$. This result occurs because the weaker the vortex flow, the stronger the effect of solar radiation. As displayed in Fig. 5b, SOSRs decrease V_{ped}/V_{inlet} under the solar angle of LST0900 (reduced by 85%) and LST1200 (reduced by 84%). Furthermore, the impact of SOSRs is complex in the isothermal condition and LST1500. In general, the influence of SOSRs on extremely deep street canyons ($H/W = 5$) is not as great as that of typical ($H/W = 1$) and deep ($H/W = 3$) street canyons.

Fig. 5c shows ΔT at the x - z central plane when $H/W = 5$ under different solar radiation conditions. SOSRs hardly changes the ΔT at LST0900 and LST1500. To better quantify and analyze the influence of SOSRs under different solar angles, Fig. 5d displays the horizontal profiles of ΔT_{ped} . Without SOSRs, ΔT_{ped} is about 1.5 °C, 2.2–3.3 °C and 2.2 °C

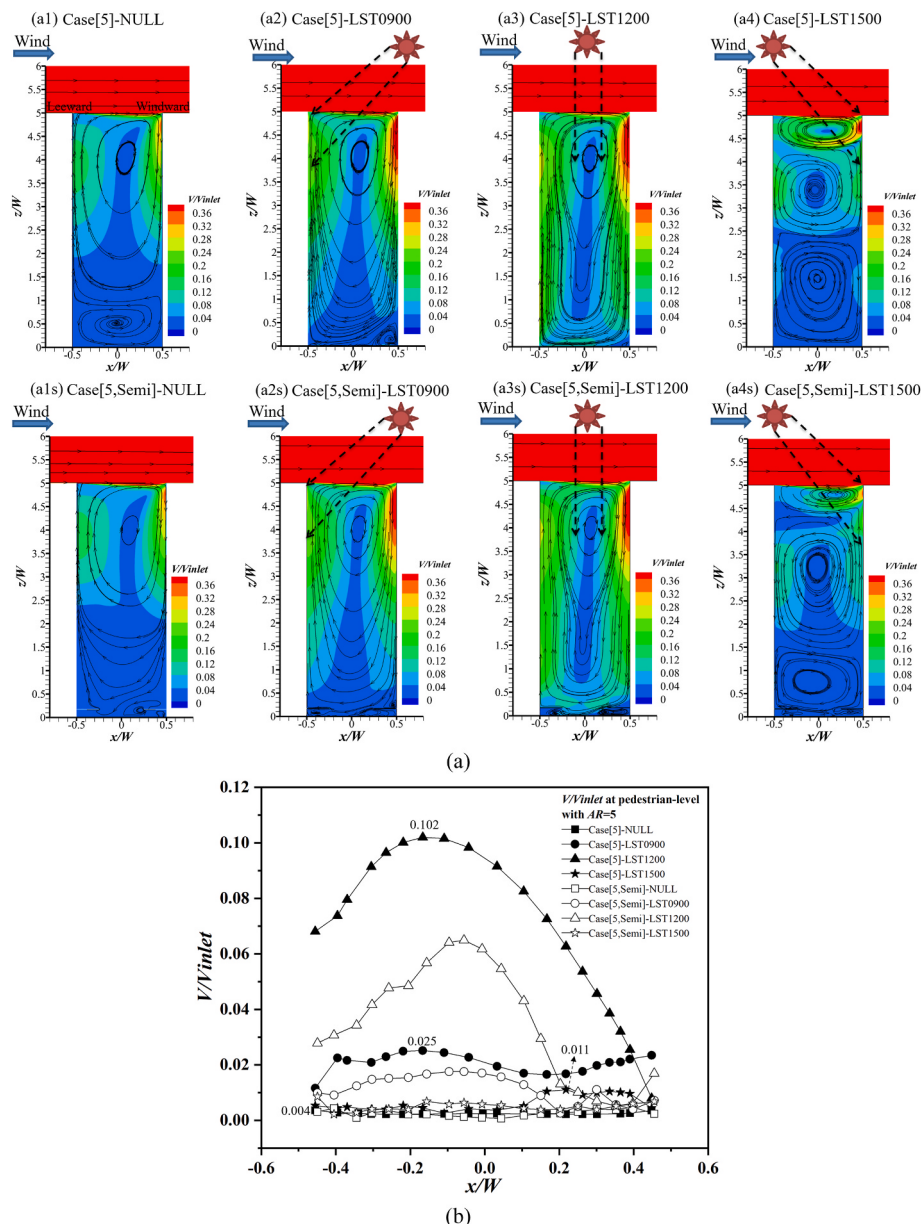


Fig. 5. In the x - z central plane for cases with/without semi-open street roofs when $H/W = 5$: (a) 2-D Streamlines and normalized velocity (V/V_{inlet}), (b) Horizontal profiles of V_{ped}/V_{inlets} (c) relative air temperature ($\Delta T = T_{air} - T_{ref}$), (d) Horizontal profiles of ΔT_{ped} .

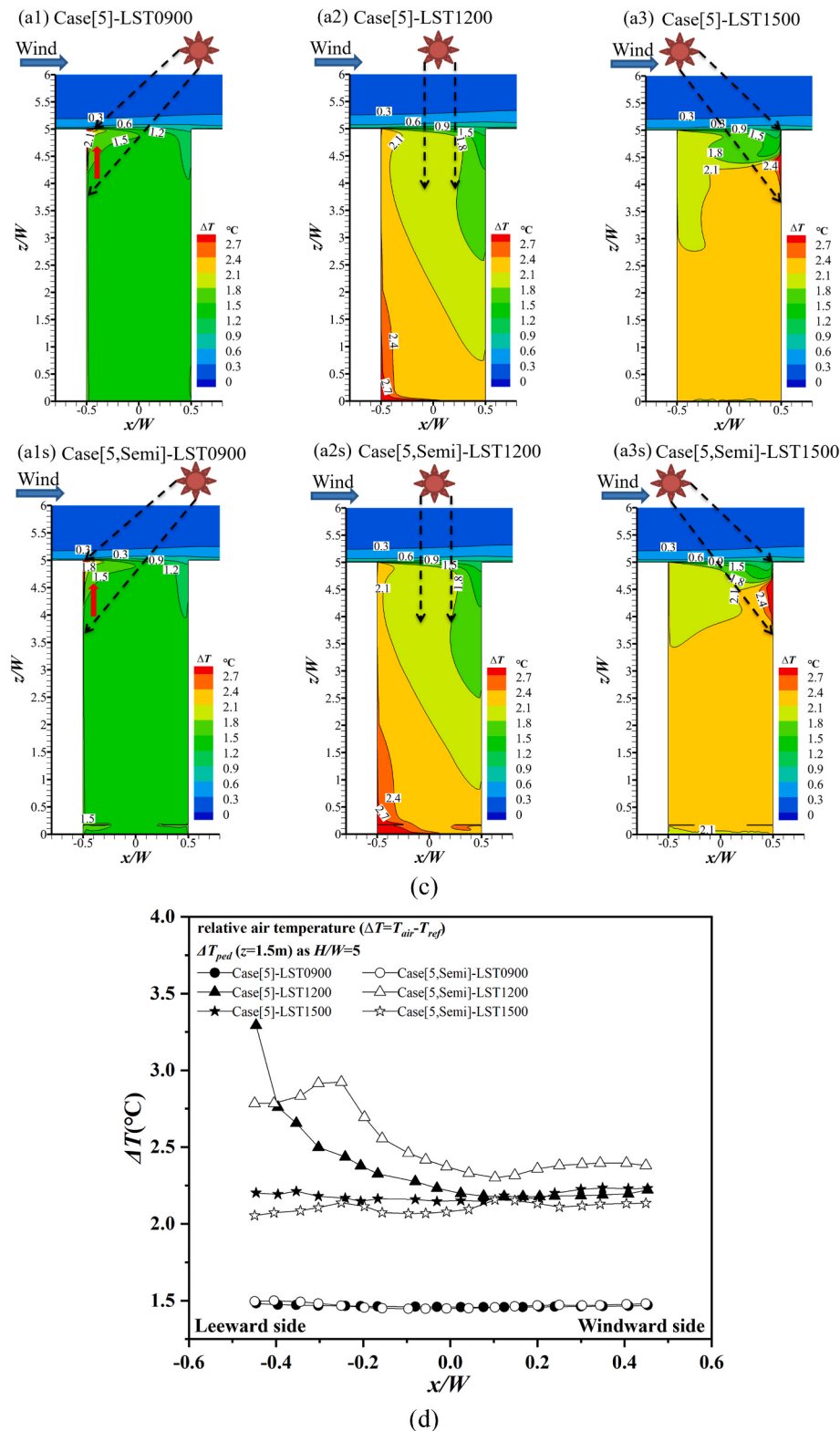


Fig. 5. (continued).

at LST0900, LST1200 and LST1500, respectively. It is close to the result when $H/W = 3$ ($\Delta T_{ped} \sim 1.4$ °C, 2–3 °C and 2.1 °C at LST0900, LST1200 and LST1500) and slightly exceed ΔT_{ped} when $H/W = 1$ (0.95–2.2 °C). With SOSRs, ΔT_{ped} changes little at LST0900 (increased by 2%) and LST1500 (decreased by 7%) while increases by 20% in most regions at LST1200 (Fig. 5d).

5.1.4. Summary of air flow and air temperature

In short, SOSRs reduce the velocity and increase the air temperatures in most pedestrian areas. In addition, its impacts on air flow and air temperature differ as the aspect ratio or solar angle changes.

For wind environment, without SOSRs, compared to the isothermal case, V_{pedmax}/V_{inlet} changes from 0.35 to 0.42, 0.44 and 0.33 when H/W

$= 1$ for LST0900, LST1200 and LST1500 cases, respectively (Fig. 3b). The V_{pedmax}/V_{inlet} varies from 0.066 to 0.074, 0.13 and 0.063 when $H/W = 3$ (Fig. 4b), confirming that LST0900 and LST1200 enhance the flow of pedestrian area slightly but LST1500 weakens airflow a little. Furthermore, for the extremely deep street canyon ($H/W = 5$), solar heating may considerably raise V_{pedmax}/V_{inlet} from 0.004 (isothermal case) to 0.025, 0.102 and 0.011 at LST0900, LST1200 and LST1500 (Fig. 5b) with 3–25 times increase. Introducing SOSRs reduces V_{ped}/V_{inlet} . In this study, installing SOSRs decreases V_{ped}/V_{inlet} from 0.33 to 0.44 to less than 0.07 when $H/W = 1$ and from 0.066 to 0.13 to <0.049 when $H/W = 3$.

As for the thermal environment, without SOSRs, ΔT_{ped} is about 0.95 °C at LST0900, 1.3–2.2 °C at LST1200 and 1.5 °C at LST1500 in typical street canyons ($H/W = 1$, see Fig. 3d). It is lower than that in deep street canyons ($H/W = 3$, pedestrian-level $\Delta T \sim 1.4$ °C, 2–3 °C and 2.1 °C at LST0900, LST1200 and LST1500 respectively, see Fig. 4d) and extremely deep street canyons ($H/W = 5$, pedestrian-level $\Delta T \sim 1.5$ °C, 2.2–3.3 °C and 2.2 °C at LST0900, LST1200 and LST1500 respectively, see Fig. 5d). The installation of SOSRs raises ΔT_{ped} . Furthermore, the effect of SOSRs on extremely deep ($H/W = 5$) street canyons is not as apparent as that on typical ($H/W = 1$) and deep ($H/W = 3$) street canyons. When $H/W = 1$, the maximum increase of ΔT_{ped} is 76% at LST0900, 152% at LST1200 and 40% at LST1500 (Fig. 3d), which is larger than that when $H/W = 3, 5$.

5.2. Impacts of aspect ratio and semi-open on outdoor thermal comfort (PET)

The impacts of SOSRs and aspect ratios on physiological equivalent temperature (PET) are discussed in this subsection. Fig. 6a–c displays PETs along a horizontal line inside a working street at the pedestrian level ($z = 1.5$ m) for typical ($H/W = 1$), deep ($H/W = 3$) and extremely deep ($H/W = 5$) street canyons with and without SOSRs under isothermal and three solar radiation conditions. According to our results, unlike 3-D urban districts, SOSRs do not significantly improve outdoor thermal comfort in most pedestrian regions of 2-D street canyons.

As shown in Fig. 6a, the horizontal profiles of PET show similar trends when $H/W = 1$ without SOSRs and thermal sensation falls at “warm” at LST0900 (average PET value~37.4 °C), “very hot” at LST1200 (average PET value~ 42.9 °C) and “hot” at LST1500 (average PET value~39.9 °C) in most pedestrian-level regions. SOSRs increase PETs under different solar radiation conditions, i.e. 3.6–5.5 °C increase at LST0900 (thermal sensation changed from “warm” to “hot”), 0.9–10.4 °C increase at LST1200 and 2.2–5.1 °C at LST1500 (thermal sensation changed from “hot” to “very hot”), respectively. This is due to the decrease in velocity (V_{ped}/V_{inlet} decreases from 0.33 to 0.44 to below 0.07) and the increase in air temperature (ΔT increases about 0.2–1.5 °C) after the installing SOSRs.

When $H/W = 3$, Fig. 6b shows that PETs vary greatly under different solar radiation conditions. Without SOSRs, the thermal sensation is estimated as “hot” at LST0900 (average PET value~41.7 °C), “very hot” at LST1200 (average PET value~48.9 °C) and “very hot” at LST1500 (average PET value~44.3 °C). The setup of SOSRs raises PET by 0.3–1.2 °C at LST0900 (thermal sensation changed from “hot” to “very hot”) and 0.1–1.1 °C at LST1500. Under the solar angle of LST1200, the setup of SOSRs largely increases PET by 1.2–4 °C. However, the PET decreases on both sidewalks (i.e. decreases by 0.8 °C and 2.5 °C for the left sidewalk and 1.4 °C for the right sidewalk). This PET reduction might be due to the shading effect of the SOSRs.

When $H/W = 5$, shown in Fig. 6c, the PETs are greater than 42 °C under three solar radiation conditions. In other words, the thermal sensation is estimated as “very hot”. It is worth mentioning that PET value hardly changes under the solar angles of LST0900 and LST1500, possibly because the building configuration provides shade rather than SOSRs. Under the solar angle of LST1200, the SOSRs increase PET in

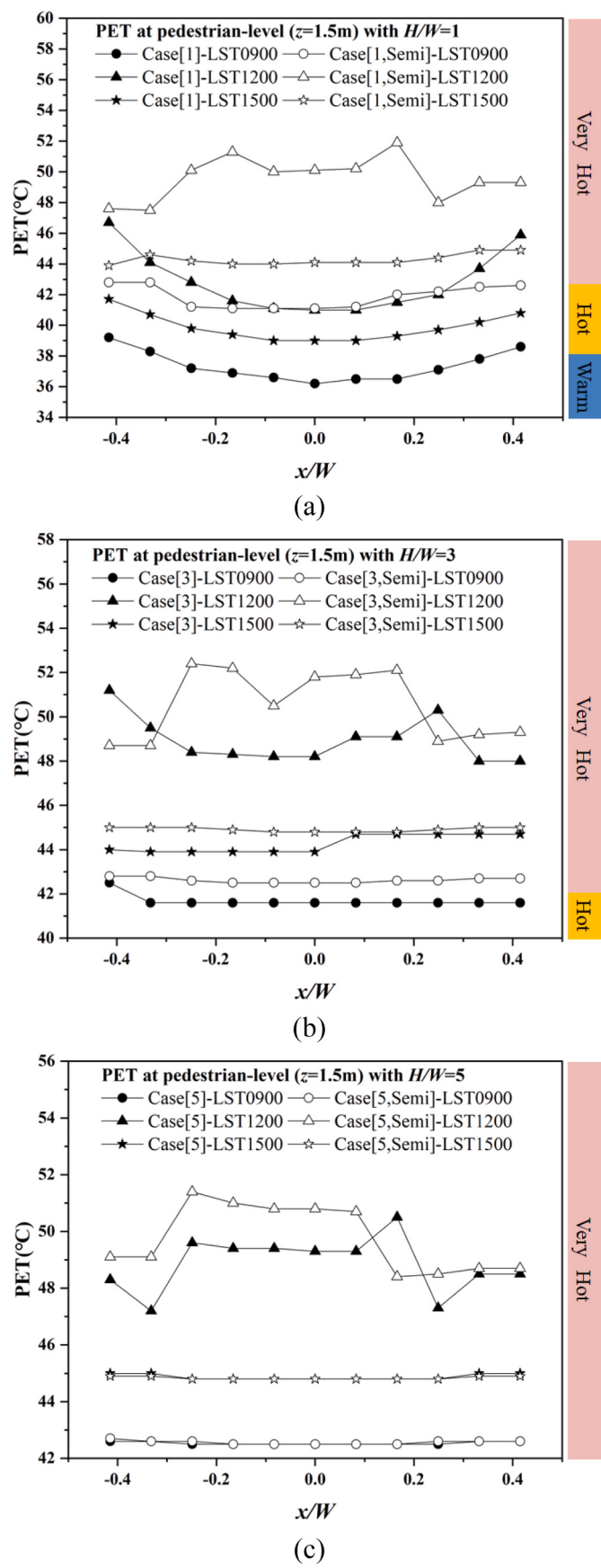


Fig. 6. PET (°C) at pedestrian level ($z = 1.5$ m) when (a) $H/W = 1$, (b) $H/W = 3$, and (c) $H/W = 5$.

most regions ($0.2\text{--}1.9$ °C). Compared to $H/W = 1,3$, the impacts of SOSRs on PET are less pronounced when $H/W = 5$. This may be because shadings do not significantly affect air temperature and wind velocity is small both with and without SOSRs (V_{ped}/V_{inlet} lower than 0.102).

5.3. Impacts of aspect ratio and semi-open on pollutant distribution and exposure

5.3.1. Impacts of aspect ratio and semi-open on pollutant distribution

This section describes the distribution characteristics of pollution under isothermal and different solar conditions with and without SOSRs. This study considers three street aspect ratios (i.e. $H/W = 1, 3, 5$). Figs. 7–9 shows pollutant CO concentration (C_{CO} , mg/m³) distributions at the central x - z plane and horizontal profiles of pedestrian-level ($z = 1.5$ m) CO concentration (C_{ped}). Note that the vehicular emission is set on the ground with a height of 0.2 m (Fig. 2b).

When $H/W = 1$, there is only one main clockwise vortex due to the flow separation at the leeward edge of the building. Without SOSRs, most pollutants will follow the near-ground airflow of the primary vortex, causing a higher concentration at the leeward-side wall (Fig. 7a). This is consistent with most studies [50]. Then, pollutants will be transported upward to the top area of the canyon with the airflow, where the air exchange and the escaping of pollutants would occur [51]. However, a significant fraction of pollutants does not transfer upwardly by vertical mean flux due to low vertical velocity [52]. In addition, solar radiation heating enhances the vortex flow and the pollutant concentration is slightly reduced. Compared with the isothermal case ($C_{ped}\sim 5.10$ mg/m³), C_{ped} is 3.83, 3.49 and 3.13 mg/m³ at LST0900, LST1200 and LST1500 respectively (Fig. 7b). After introducing the SOSRs, pollutant concentration does not have a noticeable change above the SOSRs height. However, below the SOSRs, C_{CO} at the windward-side wall increases significantly. We further analyze the pedestrian-level C_{CO}

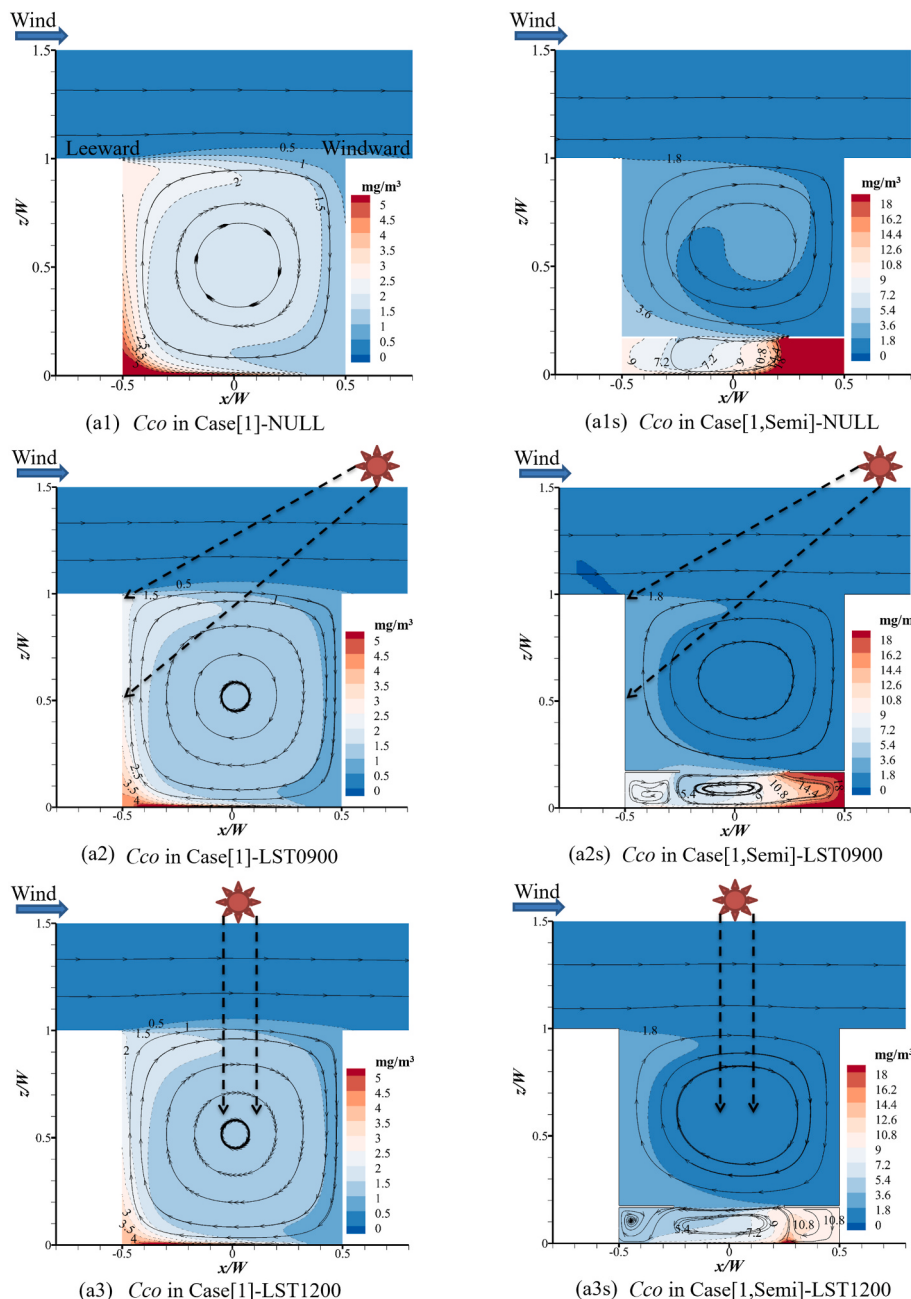


Fig. 7. Cases with/without semi-open street roofs when $H/W = 1$: (a) Streamlines and CO concentration, (b) CO concentration at pedestrian level ($z = 1.5$ m).

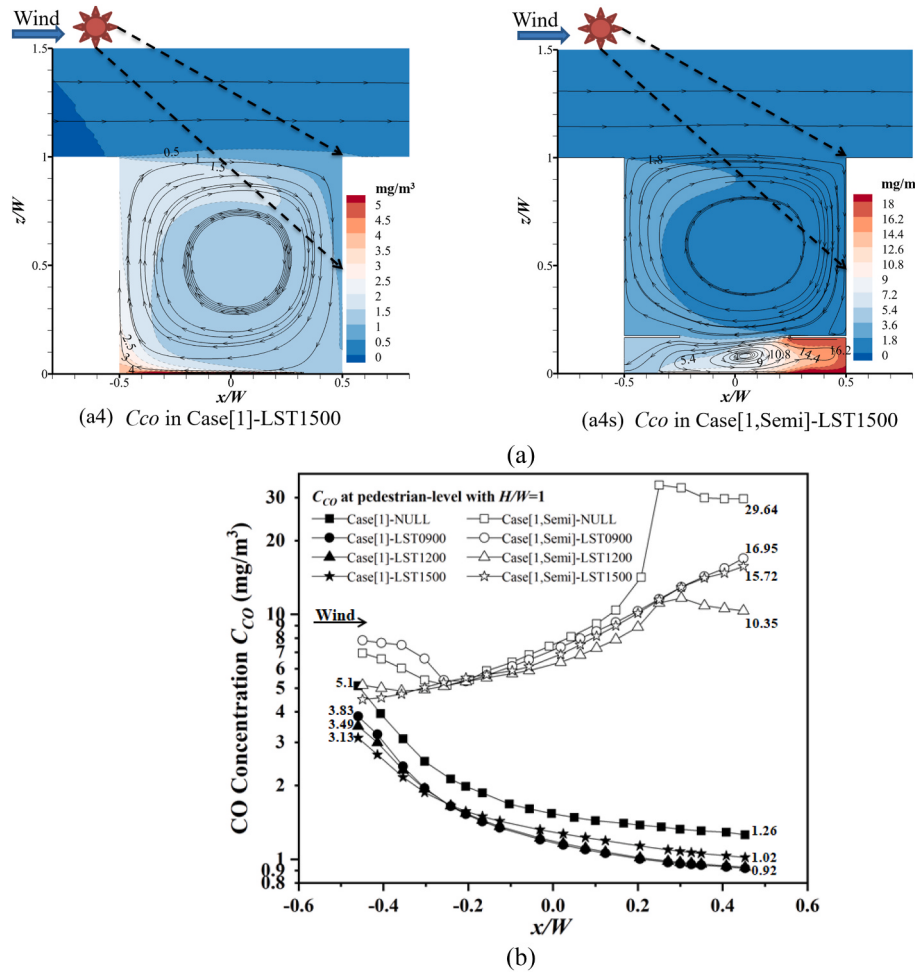


Fig. 7. (continued).

(C_{ped}) to facilitate a deeper understanding of the impact of SOSRs on pedestrian area C_{CO} , we further analyze the pedestrian-level C_{CO} (C_{ped}) as shown in Fig. 7b. The horizontal profiles reveal a steady increase from leeward-side to windward-side wall with the SOSRs. In contrast, the profiles show a reverse trend without SOSRs. Besides, SOSRs significantly enhances the windward-side C_{ped} to 12–24 times (from 1.2 mg/m^3 to 29.64 mg/m^3) and slightly raises the leeward-side C_{ped} to 1–2 times (from 3.8 mg/m^3 to 7.82 mg/m^3).

When $H/W = 3$, airflow and pollutants dispersion are affected by solar radiation. Without SOSRs, C_{CO} distributions are similar at LST0900, LST1200 and isothermal cases due to the main clockwise vortex (Fig. 8a). However, since there are two opposite vortexes at LST1500, the pollutants increase in the street canyon and the near-ground airflow transfers pollutants to the windward-side wall. In other words, C_{CO} has a larger value at the leeward-side wall than the windward-side wall, except at LST1500. In addition, compared with the isothermal condition ($C_{ped} \sim 19.15 \text{ mg}/\text{m}^3$, see Fig. 8b), pollutants decrease at LST0900 ($C_{ped} \sim 6.98 \text{ mg}/\text{m}^3$) and LST1200 ($C_{ped} \sim 5.49 \text{ mg}/\text{m}^3$). With the SOSRs, pollutants are mainly distributed below the SOSRs height due to the airflow. Fig. 8b displays the horizontal profiles of C_{ped} . After installing SOSRs, at the windward-side wall, C_{ped} is about 7–43 times larger than that without the SOSRs at LST0900, LST1200 and isothermal case (Fig. 8b). At LST1500, SOSRs slightly raises the windward-side C_{ped} from 10.42 mg/m^3 to 13.44 mg/m^3 . At the leeward-side wall, C_{ped} decreases at the isothermal (from 19.15 to 12.76 mg/m^3) condition. However, it increases at LST0900 (from 6.98 to 12.76 mg/m^3) and LST1500 (from 2.72 to 30.57 mg/m^3) conditions due to the setup of the SOSRs.

When $H/W = 5$, Fig. 9a shows that solar radiation (LST0900 and LST1200) significantly reduces the pollutant concentration near the ground compared with the isothermal case ($C_{ped} \sim 62.03 \text{ mg}/\text{m}^3$). The reduction of the pollution concentration is the strongest under the solar angle of LST1200 ($C_{ped} \sim 7.09 \text{ mg}/\text{m}^3$), followed by LST0900 ($C_{ped} \sim 13.57 \text{ mg}/\text{m}^3$). With SOSRs, the pollutants beneath the SOSRs height increases significantly. To better evaluate the impacts of SOSRs on pedestrian-level C_{CO} , Fig. 9b displays C_{CO} at pedestrian-level height ($z = 1.5$ m). With solar radiation heating, SOSRs enhance pollutant accumulation. C_{ped} increases most at the LST1500 case (from 12.60 mg/m^3 to 168.09 mg/m^3 , 13 times), followed by the LST0900 case (from 4.65 mg/m^3 to 50.93 mg/m^3 , about 11 times), and the growth is the least at LST1200 (from 2.62 mg/m^3 to 22.30 mg/m^3 , about 6 times). However, as displayed in Fig. 9b, the SOSRs reduce C_{ped} in most regions except at the leeward-side wall in the isothermal case (from 62.03 mg/m^3 to 104.13 mg/m^3).

5.3.2. Impacts of aspect ratio and semi-open on pollutant exposure

The urban street canyon is where vehicle exhaust is emitted and dispersed, causing exposure of residents to these pollutants [51]. Figs. 10–12 displays the personal intake fraction (P_{IF}) vertical profiles for the residents living in near-road buildings at the leeward-side and windward-side wall when $H/W = 1, 3, 5$. In a word, first-floor P_{IF} is significantly larger than the higher-floor. P_{IF} and personal intake fraction differ when the aspect ratio and solar angle change. SOSRs significantly influence the lower-floor P_{IF} .

When $H/W = 1$, Fig. 10a displays the leeward-side P_{IF} ($\langle P_{IF} \rangle_{lee}$) with and without SOSRs. The $\langle P_{IF} \rangle_{lee}$ decreases with the increase of

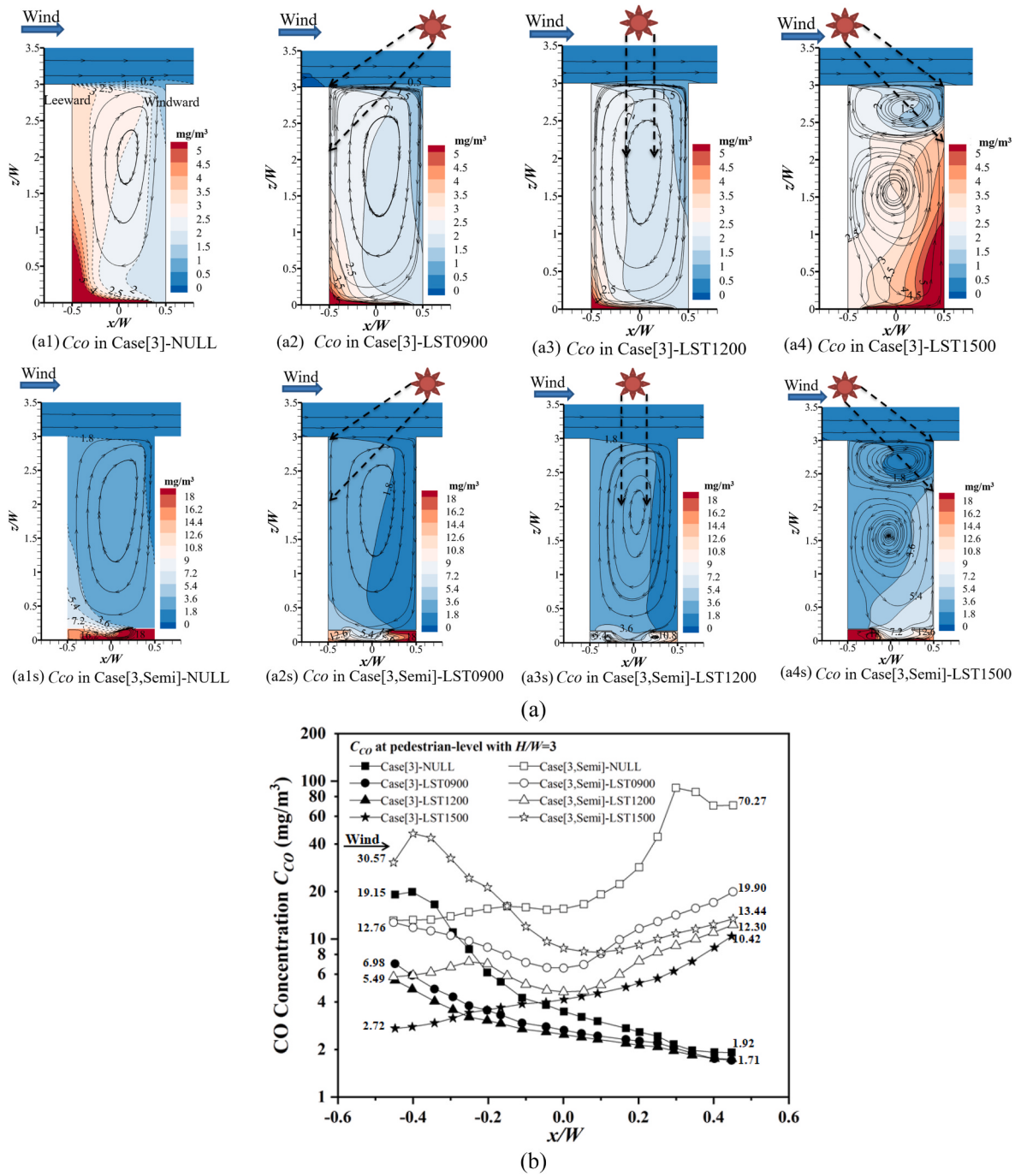


Fig. 8. Cases with/without semi-open street roofs when $H/W = 3$: (a) Streamlines and CO concentration, (b) CO concentration at pedestrian level ($z = 1.5$ m).

floors and solar radiation reduces $\langle P_{IF} \rangle_{lee}$. When SOSRs are installed, first-floor $\langle P_{IF} \rangle_{lee}$ increased significantly at LST0900 (from 7.37 ppm to 16.37 ppm), LST1200 (from 6.88 ppm to 10.46 ppm), LST1500 (from 6.11 ppm to 8.71 ppm) and isothermal case (from 10.01 ppm to 18.29 ppm). However, higher-floor $\langle P_{IF} \rangle_{lee}$ changes relatively slightly, especially under the solar angle of LST1200. Fig. 10b depicts the windward-side P_{IF} ($\langle P_{IF} \rangle_{wind}$) with and without SOSRs. The setup of SOSRs changes higher-floor $\langle P_{IF} \rangle_{wind}$ slightly. Compared with the leeward-side (Fig. 10a), SOSRs raise windward-side P_{IF} ($\langle P_{IF} \rangle_{wind}$) more obviously on the first floor. In particular, $\langle P_{IF} \rangle_{wind}$ increases from 1.79 ppm to 37.30 ppm at LST0900, from 1.81 ppm to 20.38 ppm at LST1200, from 1.99 ppm to 35.14 ppm at LST1500 and from 2.44 ppm to 76.06 ppm at isothermal case (Fig. 10b). Besides, $\langle P_{IF} \rangle_{lee}$ is larger than $\langle P_{IF} \rangle_{wind}$ without the SOSRs, while the situation is reverse

after introducing the SOSRs.

When $H/W = 3$, SOSRs raise $\langle P_{IF} \rangle_{lee}$ slightly except for the first floor under three different solar radiation conditions (Fig. 11a). For the first floor, $\langle P_{IF} \rangle_{lee}$ grows up to about 2 times at LST0900 (from 13.46 ppm to 27.87 ppm), 11 times at LST1500 (from 5.35 ppm to 62.03 ppm) after installing the SOSRs. Under the solar angle of LST1200, $\langle P_{IF} \rangle_{lee}$ hardly changes on the first floor. It is worth mentioning that, in the isothermal case, $\langle P_{IF} \rangle_{lee}$ decreases after installing SOSRs (first-floor $\langle P_{IF} \rangle_{lee}$ decreases from 44.87 ppm to 30.71 ppm). Fig. 11b displays the vertical profiles of $\langle P_{IF} \rangle_{wind}$ in deep street canyon ($H/W = 3$). SOSRs hardly impact higher-floor $\langle P_{IF} \rangle_{wind}$ at LST0900, LST1200 and the isothermal case. However, under the solar angle of LST1500, SOSRs reduce higher-floor $\langle P_{IF} \rangle_{wind}$. This reduction is mainly due to the accumulation of pollutants below the semi-open height (Fig. 8a). For the

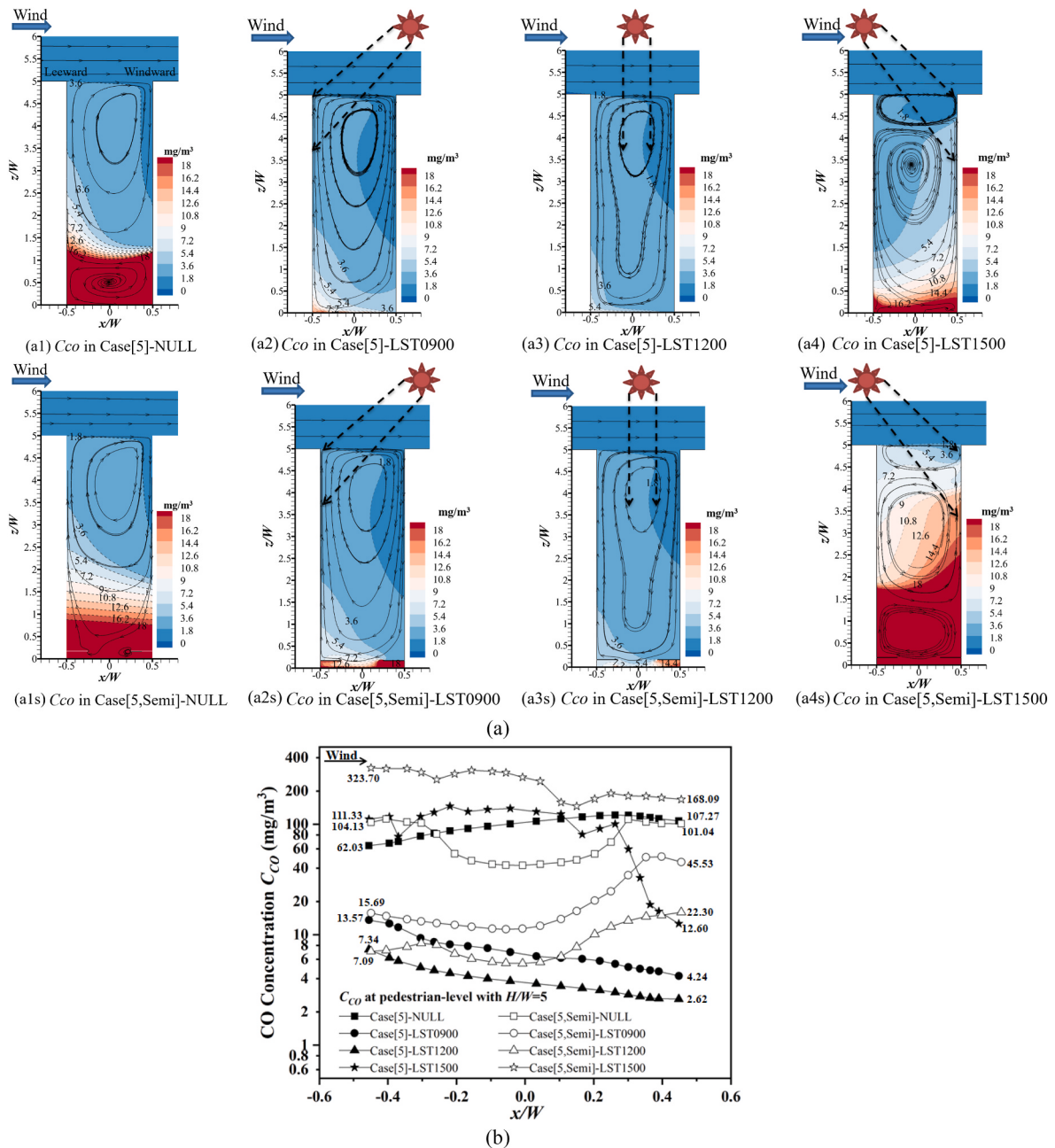


Fig. 9. Cases with/without semi-open street roofs when $H/W = 5$: (a) Streamlines and CO concentration, (b) CO concentration at pedestrian level ($z = 1.5 \text{ m}$).

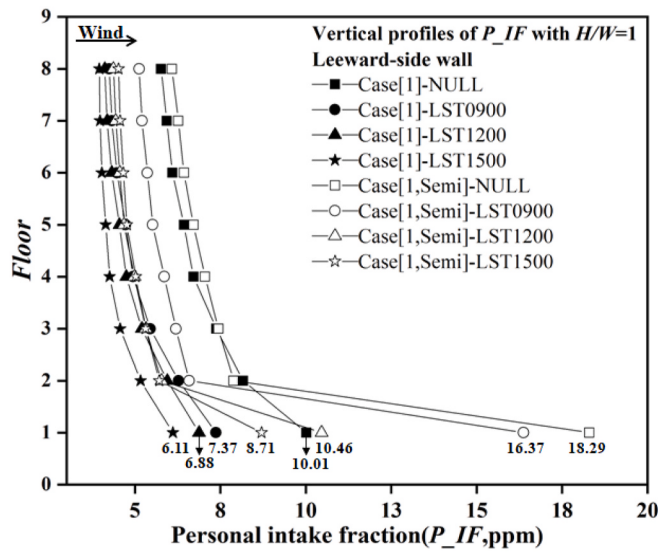
first floor, SOSRs increase $\langle P_{IF} \rangle_{wind}$ by 13 times at LST0900 (from 3.39 ppm to 43.8 ppm), 7 times at LST1200 (from 3.5 ppm to 25.18 ppm) and 33 times at isothermal case (from 3.92 ppm to 131.47 ppm). At LST1200, first-floor $\langle P_{IF} \rangle_{wind}$ changes slightly, i.e. from 22.67 ppm to 28.32 ppm.

When $H/W = 5$, Fig. 12a displays the vertical profiles of $\langle P_{IF} \rangle_{lee}$ with and without SOSRs. SOSRs decrease the 2nd to 20th $\langle P_{IF} \rangle_{lee}$ at LST0900, LST1200 conditions, and isothermal case. At LST1500, the setup of SOSRs impacts $\langle P_{IF} \rangle_{lee}$ complexly, as $\langle P_{IF} \rangle_{lee}$ increases on the 17th to 40th floor while decreasing on most lower floors. For the first floor, $\langle P_{IF} \rangle_{lee}$ increases by 7.92 ppm (from 27.37 ppm to 35.29 ppm) at LST0900, 377.76 ppm at LST1500 (from 219.82 ppm to 597.58 ppm) and 85.59 ppm at isothermal case (from 119.73 ppm to 205.32 ppm). However, the first-floor $\langle P_{IF} \rangle_{lee}$ decreases by 1.64 ppm at LST1200, i.e. from 15.61 ppm to 13.97 ppm. As depicted in Fig. 12b, the change of higher-floor $\langle P_{IF} \rangle_{wind}$ is fairly small at LST0900 and LST1200 with and

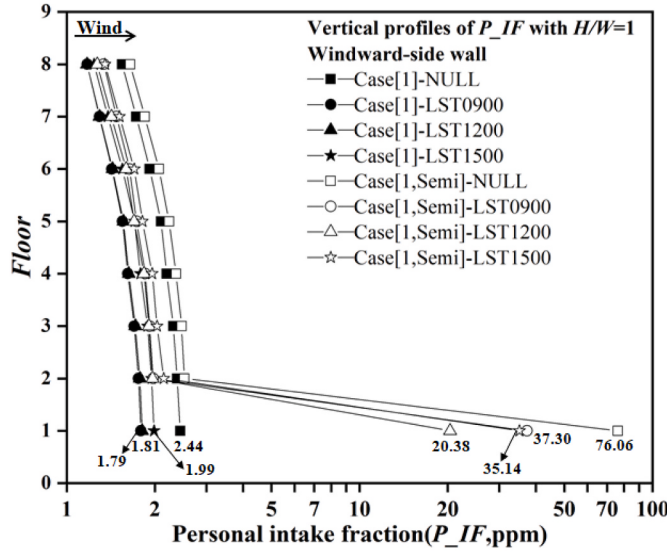
without SOSRs. However, under the solar angle of LST1500, SOSRs significantly increase $\langle P_{IF} \rangle_{wind}$ at the higher floor, and the situation is relatively complex in the isothermal case. For the first floor, the setup of SOSRs raises $\langle P_{IF} \rangle_{wind}$ up to 9 times (from 8.73 ppm to 78.18 ppm) at LST0900, 6 times (from 5.19 ppm to 31.92 ppm) at LST1200 and 10 times (from 31.92 ppm to 301.24 ppm) at LST1500 compared the ones without SOSRs. For the isothermal case, the first-floor $\langle P_{IF} \rangle_{wind}$ decreases slightly, namely from 207 ppm to 119.73 ppm with SOSRs.

5.3.3. Summary of pollutant dispersion and pollutant exposure

In brief, the simulation results confirm that SOSRs reduce the wind speed within the street canyon, leading to an accumulation of pollutant concentrations. Besides, the effect of SOSRs is related to aspect ratios and solar angles conditions. In street canyons that are perpendicular to the incoming wind direction, vortices inside the street could restrict pollutant transmission, resulting in a high pollutant concentration inside



(a)

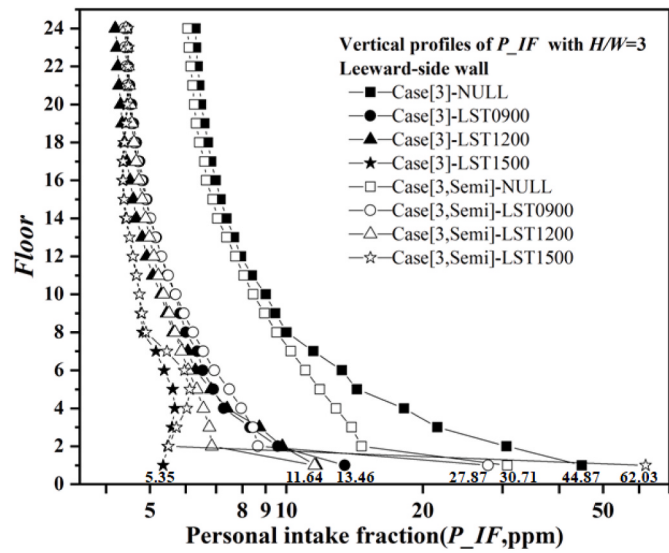


(b)

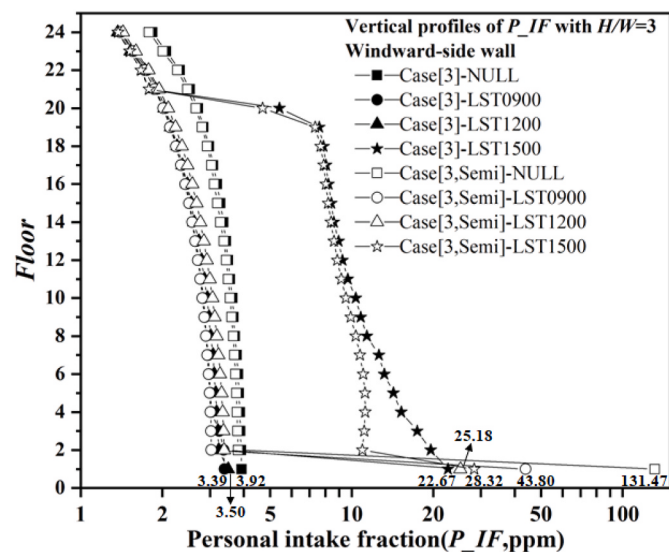
Fig. 10. The vertical profiles of personal intake fraction (P_{IF} , ppm) when $H/W = 1$: (a) leeward-side wall, (b) windward-side wall.

the urban street canyon [51]. Without SOSRs, when $H/W = 1$, there is only one main clockwise vortex and most pollutants will follow the airflow, thus leading to a higher concentration at the leeward-side wall. This finding is consistent with previous literature [50]. For deep street canyons, the airflow inside the street canyon would be much more complex with a single vortex or multi-vortices [51]. When $H/W = 3$, pollutants dispersion situations are similar to the typical street canyon ($H/W = 1$) under three solar angles cases (LST0900, LST1200 and isothermal case), while pollutants are increased and transported to the windward-side wall due to two opposite vortexes are formed at LST1500. When $H/W = 5$, one main clockwise is formed at LST0900 and LST1200, thus leading to the pollutant concentrations near the leeward-side wall being higher than the windward-side wall. Instead, three vortices are formed at LST1500 and pollutants accumulate on the windward-side wall.

SOSRs weaken the air circulation inside the street canyon, causing an accumulation of high pollutant concentration in the pedestrian area in the street canyon. When $H/W = 1$, SOSRs significantly enhance the windward-side C_{ped} to 12–24 times and slightly raise the leeward-side



(a)



(b)

Fig. 11. The vertical profiles of personal intake fraction (P_{IF} , ppm) when $H/W = 3$: (a) leeward-side wall, (b) windward-side wall.

C_{ped} to 1–2 times. When $H/W = 3$, the windward-side C_{ped} is about 7–43 times larger than that without the SOSRs at LST0900, LST1200 and isothermal case. At LST1500, SOSRs slightly raises the windward-side C_{ped} (from 10.42 mg/m^3 to 13.44 mg/m^3) and significantly enhances the leeward-side C_{ped} (from 2.72 mg/m^3 to 30.57 mg/m^3). When $H/W = 5$, C_{ped} increases most at LST1500 case (13 times), followed by LST0900 case (11 times), and the growth is the least at LST1200 (6 times). However, in most regions, SOSRs reduce C_{ped} in most regions except at the leeward-side wall in the isothermal case (from 62.03 mg/m^3 to 104.13 mg/m^3).

To better understand the characteristics of pollutants exposure, Fig. 13 shows the spatially-averaged P_{IF} ($\langle P_{IF} \rangle$) at both sides of the canyons. For cases without SOSRs, $\langle P_{IF} \rangle$ is 4.6 ppm, 3.4 ppm, 3.2 ppm and 3.2 ppm at the isothermal condition, LST0900, LST1200 and LST1500 respectively in typical street canyons ($H/W = 1$). SOSRs increase $\langle P_{IF} \rangle$ up to 1.5–2.1 times when $H/W = 1$. For cases without SOSRs in deep street canyons ($H/W = 3$), $\langle P_{IF} \rangle$ is 1.26–2.28 times higher than that in typical street canyons, which is 7.5 ppm, 4.3 ppm, 4.1 ppm and 7.3 ppm at isothermal condition, LST0900, LST1200 and

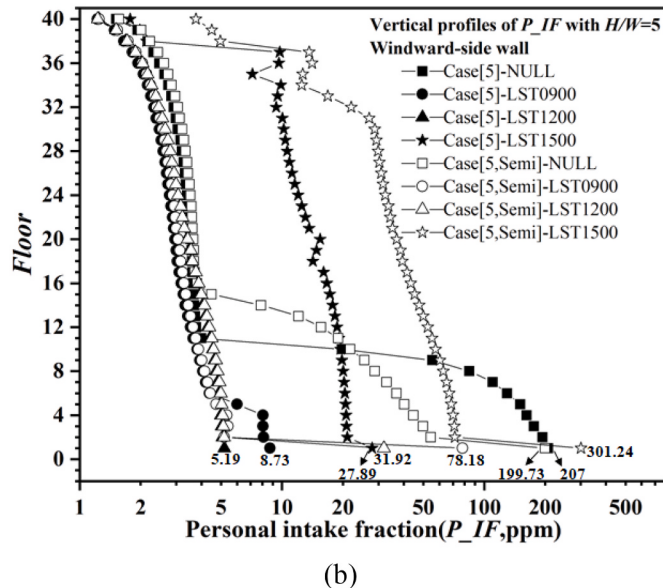
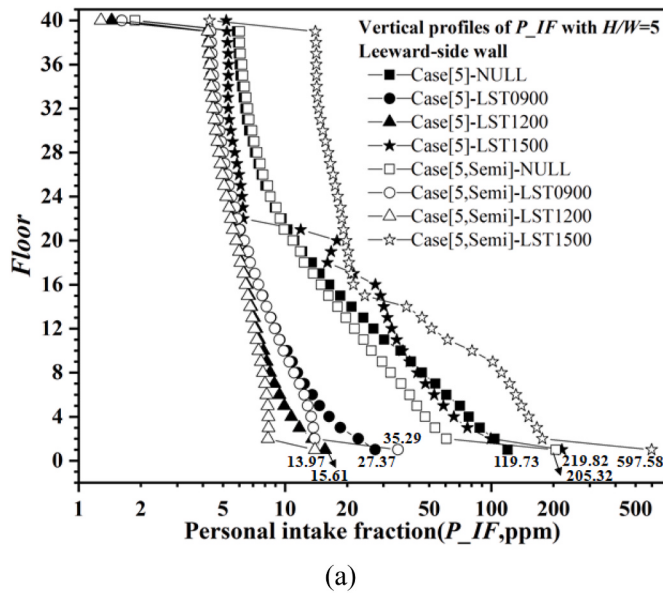


Fig. 12. The vertical profiles of personal intake fraction (P_{IF} , ppm) when $H/W = 5$: (a) leeward-side wall, (b) windward-side wall.

LST1500 respectively. When $H/W = 3$, SOSRs raise $\langle P_{IF} \rangle$ up to 1.1–1.3 times. For extremely deep street canyons ($H/W = 5$), without SOSRs, compared to LST0900 ($\langle P_{IF} \rangle \sim 5.9$ ppm) and LST1200 ($\langle P_{IF} \rangle \sim 5$ ppm) situations, $\langle P_{IF} \rangle$ is larger at isothermal condition (30.1 ppm) and LST1500 (21.1 ppm) due to the airflow. When $H/W = 5$, $\langle P_{IF} \rangle$ increases by 1.02–2.49 times with SOSRs under three solar radiation conditions, i.e. from 5 ppm to 5.1 ppm, from 5.9 ppm to 6.5 ppm and from 21.1 ppm to 52.6 ppm at LST0900, LST1200 and LST1500. However, SOSRs decrease $\langle P_{IF} \rangle$ from 30.1 ppm to 19.4 ppm in the isothermal case.

5.4. Limitation and future work

In this study, the SOSRs significantly reduce pedestrian-level velocity in 2-D idealized street canyons. It is worth mentioning that 2-D street canyon corresponds to worse ventilation than 3-D urban models because only vertical exchange and turbulent fluxes across street roof that contribute to 2-D street canyon ventilation. At the same time, there is lateral ventilation for the 3-D street canyon. We will consider the

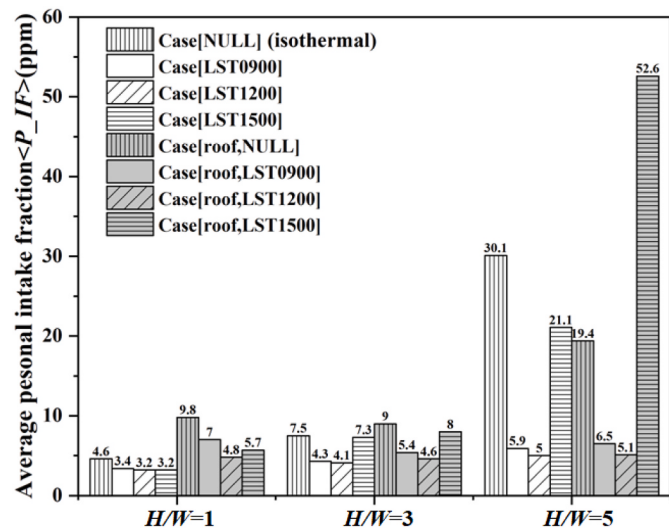


Fig. 13. The spatially-averaged P_{IF} ($\langle P_{IF} \rangle$, ppm) of CO at both sides of the canyon when $H/W = 1, 3, 5$.

influencing mechanisms of SOSRs, solar radiation heating, aspect ratios in more complicated 2-D and 3-D urban models in the future.

Besides, this study applies only one shading strategy. However, cities are more complicated with multiple types of SOSRs. For example, Kwon et al. [53] demonstrated that a flexible canopy played a crucial role in increasing outdoor thermal comfort under the canopy area. Flexible architectural elements such as blinds or canopies, can be beneficial for controlling the building environment. Thus, future studies can consider the effect of various shading strategies on the microclimate in urban street canyons.

Finally, CFD validation will be further conducted under the estimation of scaled outdoor measurement in recent literature [54–56], in which radiation processes, turbulence characteristics and high-resolution air/wall temperature are all measured. We are conducting scaled outdoor experimental studies of urban turbulence and thermal environment coupling turbulence and radiation processes in street canyon models with or without semi-open street roofs (SOSRs). These scaled outdoor experiments consider various aspect ratios and semi-open street roofs (Fig.A3). The results will be presented in future studies, which have rarely been investigated.

6. Conclusions

Semi-open street roofs (SOSRs) have been demonstrated to provide solar shading for pedestrians in three-dimensional (3-D) urban districts, typically improving pedestrian-level outdoor thermal comfort but weakening urban ventilation and raising pollutant exposure. However, the literature has only evaluated these positive and negative impacts separately, and their integrated impacts have rarely been quantified. In particular, some realistic urban districts comprise street canyons with tall buildings can be simplified as two-dimensional (2-D) models, which are assumed to experience the worst ventilation with a perpendicular approaching wind direction to the street axis. These negative and positive impacts of SOSRs in 2-D streets have not been investigated.

Therefore, this study performed computational fluid dynamics (CFD) simulations to simultaneously investigate the impact of semi-open street roofs (SOSRs) on both outdoor thermal environment and pollutant exposure in typical ($H/W = 1$), deep ($H/W = 3$) and extremely deep ($H/W = 5$) 2-D full-scale street canyons. Besides, our simulations were conducted under isothermal and three solar radiation conditions (LST0900, LST1200, and LST1500). The major results are summarized as follows:

- (1) Only one main clockwise vortex exists when $H/W = 1$ and 3. The SOSRs may produce some secondary clockwise and counter-clockwise vortexes at the pedestrian level, thus significantly reducing V_{ped}/V_{inlet} . When $H/W = 1$, the V_{maxped}/V_{inlet} with four solar conditions decreases from 0.33–0.44 to below 0.07 if the SOSRs are installed. When $H/W = 3$, the SOSRs can reduce V_{maxped}/V_{inlet} from 0.063–0.13 to 0.049. When $H/W = 5$, without SOSRs, two main vortexes appear in the isothermal case with V_{maxped}/V_{inlet} of only 0.004, and three solar angles raise V_{maxped}/V_{inlet} to 3–25 times. The impact of SOSRs for $H/W = 5$ is much less significant than that for $H/W = 1$ and $H/W = 3$.
- (2) The setup of SOSRs raises the pedestrian-level ΔT . ΔT_{ped} with SOSRs is 1.2–2.5 times ($H/W = 1$), 1.1–1.5 times ($H/W = 3$) higher than that without SOSRs. However, its effect on extremely deep ($H/W = 5$) street canyons is unimportant.
- (3) Unlike 3-D urban districts, SOSRs do not improve outdoor thermal comfort in most pedestrian regions of 2-D street canyons. SOSRs significantly increase pedestrian-level PETs by 0.9–10.4 °C when $H/W = 1$ and by 0.1–4 °C when $H/W = 3$. When $H/W = 5$, SOSRs raise the pedestrian-level PET by only 0.2–1.9 °C at LST1200 and hardly change at LST0900 and LST1500.
- (4) SOSRs significantly raise pedestrian-level pollutants concentration but only increase overall pollutants exposure ($\langle P_{IF} \rangle$) to 1.5–2.1 times when $H/W = 1$ and 1.1–1.3 times when $H/W = 3$. When $H/W = 5$, $\langle P_{IF} \rangle$ increases by 1.02–2.49 times with SOSRs under three solar radiation conditions.

Further investigations are still required to provide a guideline for applying SOSRs in urban areas to improve outdoor thermal comfort in hot summer. Our study indicates that the applications of SOSRs significantly worsen pedestrian-level thermal comfort in hot summer and raise pollutant exposure in present 2-D street canyons ($H/W = 1, 3, 5$), which differs from the positive impacts in 3-D urban models reported in the literature. Therefore, the impacts of semi-open street roofs vary for different urban models and should be evaluated before their application.

APPENDIX A

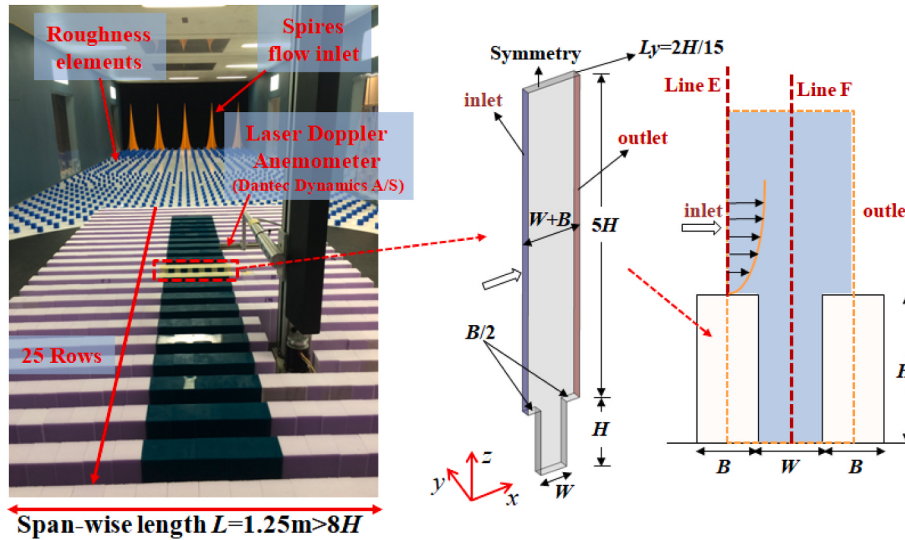


Fig. A1. The photos of wind tunnel experiments and full-scale CFD domain and boundary conditions.

CRediT authorship contribution statement

Huiru Zhong: Writing – review & editing, Writing – original draft, Visualization, Software, Methodology, Formal analysis, Data curation, Conceptualization. **Jiaxi Feng:** Visualization, Software, Methodology, Formal analysis, Data curation, Conceptualization. **Cho Kwong Charlie Lam:** Writing – review & editing, Methodology, Investigation, Conceptualization. **Jian Hang:** Writing – review & editing, Writing – original draft, Validation, Project administration, Methodology, Investigation, Formal analysis, Conceptualization. **Jiajia Hua:** Writing – review & editing. **Zhongli Gu:** Writing – review & editing.

Declaration of competing interest

The authors declare that they have no known competing financial interests or personal relationships that could have appeared to influence the work reported in this paper.

Data availability

Data will be made available on request.

Acknowledgment

This study is supported by the National Natural Science Foundation of China (No. 42175095, 41875015, and 41905005), Guangdong Major Project of Basic and Applied Basic Research (2020B0301030004, 2021B0301030007), as well as Guangdong Province Key Laboratory for Climate Change and Natural Disaster Studies (Grant 2020B1212060025), the Innovation Group Project of Southern Marine Science and Engineering Guangdong Laboratory (No. 311020001). The CFD simulations of this research were conducted on the Tianhe II supercomputer at the National Supercomputer Center, Guangzhou, P.R. China.

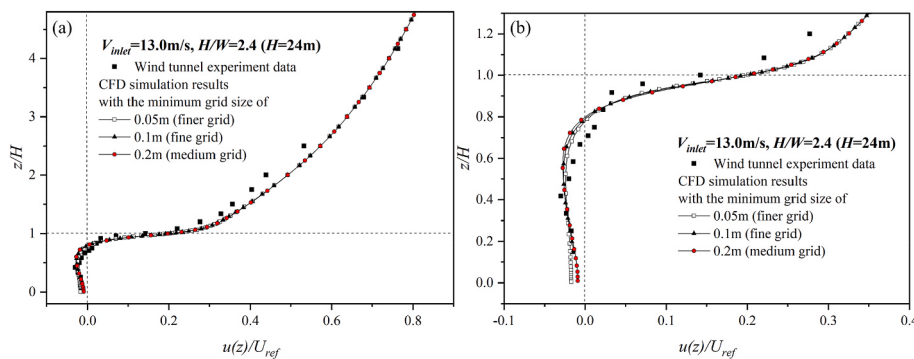


Fig. A2. (a)The comparison of CFD results and wind tunnel data for stream-wise velocity profiles at Line F; (b) partial enlargement of the left figure.

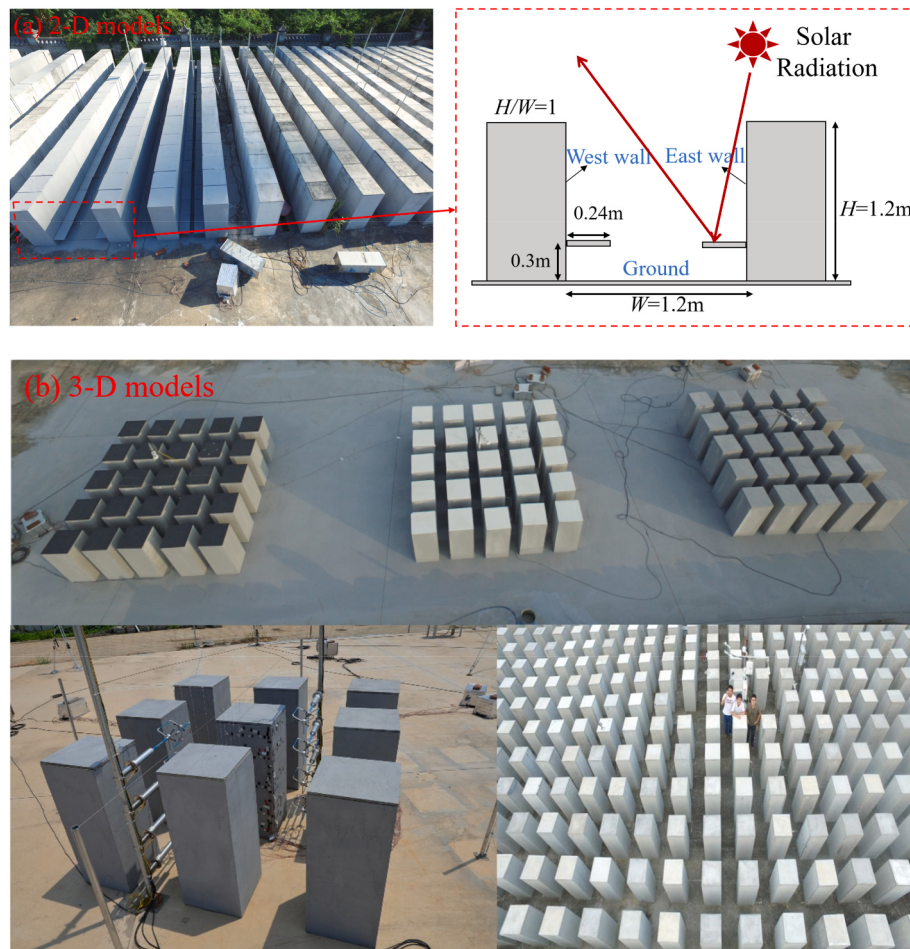


Fig. A3. (a) 2-D street canyon models in SOMUCH scaled outdoor experiments; (b) 3-D building cluster models in SOMUCH scaled outdoor experiments.

References

- [1] W.T.L. Chow, M. Roth, Temporal dynamics of the urban heat island of Singapore, *Int. J. Climatol.* 26 (15) (2006) 2243–2260, <https://doi.org/10.1002/joc.1364>.
- [2] J. Tan, Y. Zheng, X. Tang, C. Guo, L. Li, G. Song, X. Zhen, D. Yuan, A.J. Kalkstein, F. Li, The urban heat island and its impact on heat waves and human health in Shanghai, *Int. J. Biometeorol.* 54 (1) (2010) 75–84, <https://doi.org/10.1007/s00484-009-0256-x>.
- [3] J.H. Tibbatts, Air quality and climate change: a delicate balance, *Environ. Health Perspect.* 123 (6) (2015) A148–A153, <https://doi.org/10.1289/ehp.123-A148>.
- [4] Z. Luo, Y. Li, W.W. Nazaroff, Intake fraction of nonreactive motor vehicle exhaust in Hong Kong, *Atmos. Environ.* 44 (15) (2010) 1913–1918, <https://doi.org/10.1016/j.atmosenv.2010.02.016>.
- [5] X. Xie, C.-H. Liu, D.Y.C. Leung, Impact of building facades and ground heating on wind flow and pollutant transport in street canyons, *Atmos. Environ.* 41 (39) (2007) 9030–9049, <https://doi.org/10.1016/j.atmosenv.2007.08.027>.
- [6] D. Lai, W. Liu, T. Gan, K. Liu, Q. Chen, A review of mitigating strategies to improve the thermal environment and thermal comfort in urban outdoor spaces, *Sci. Total Environ.* 661 (2019) 337–353, <https://doi.org/10.1016/j.scitotenv.2019.01.062>.
- [7] C.K.C. Lam, H. Lee, S.-R. Yang, S. Park, A review on the significance and perspective of the numerical simulations of outdoor thermal environment, *Sustain. Cities Soc.* 71 (2021), 102971, <https://doi.org/10.1016/j.scs.2021.102971>.
- [8] S. Shoshtarian, P. Rajagopalan, A. Sagoo, A comprehensive review of thermal adaptive strategies in outdoor spaces, *Sustain. Cities Soc.* 41 (2018) 647–665, <https://doi.org/10.1016/j.scs.2018.06.005>.
- [9] M. Elhababi, N. Hamza, Outdoor thermal comfort: coupling microclimatic parameters with subjective thermal assessment to design urban performative

- spaces, *Buildings* 10 (12) (2020) 238, <https://doi.org/10.3390/buildings10120238>.
- [10] I. Lee, J. Voogt, T. Gillespie, Analysis and comparison of shading strategies to increase human thermal comfort in urban areas, *Atmosphere* 9 (3) (2018) 91, <https://doi.org/10.3390/atmos9030091>.
 - [11] R. Paolini, A.G. Mainini, T. Poli, L. Vercesi, Assessment of thermal stress in a street canyon in pedestrian area with or without canopy shading, *Energy Proc.* 48 (2014) 1570–1575, <https://doi.org/10.1016/j.egypro.2014.02.177>.
 - [12] A. Peeters, L. Shashua-Bar, S. Meir, R.R. Shmulevich, Y. Caspi, M. Weyl, W. Motzafi-Haller, N. Angel, A decision support tool for calculating effective shading in urban streets, *Urban Clim.* 34 (2020), <https://doi.org/10.1016/j.ulclim.2020.100672>.
 - [13] N. Nasrollahi, Y. Namazi, M. Taleghani, The effect of urban shading and canyon geometry on outdoor thermal comfort in hot climates: a case study of Ahvaz, Iran, *Sustain. Cities Soc.* 65 (2021), <https://doi.org/10.1016/j.scs.2020.102638>.
 - [14] C.K.C. Lam, J. Weng, K. Liu, J. Hang, The effects of shading devices on outdoor thermal and visual comfort in Southern China during summer, *Build. Environ.* (2022), <https://doi.org/10.1016/j.buildenv.2022.109743>.
 - [15] L.S.H. Lee, P.K. Cheung, C.K.W. Fung, C.Y. Jim, Improving street walkability: biometeorological assessment of artificial-partial shade structures in summer sunny conditions, *Int. J. Biometeorol.* 64 (4) (2020) 547–560, <https://doi.org/10.1007/s00484-019-01840-9>.
 - [16] C. Kwon, K. Lee, Outdoor Thermal comfort in a transitional space of canopy in schools in the UK, *Sustainability* 9 (10) (2017) 1753, <https://doi.org/10.3390/su9101753>.
 - [17] Z. Tan, A. Wang, T.E. Morakinyo, E.H.K. Yung, E.H.W. Chan, Assessing the mitigation performance of building setback from street and the combination with roadside tree planting, *Build. Environ.* 212 (2022), <https://doi.org/10.1016/j.buildenv.2022.108814>.
 - [18] J. Hang, Z. Luo, M. Sandberg, J. Gong, Natural ventilation assessment in typical open and semi-open urban environments under various wind directions, *Build. Environ.* 70 (2013) 318–333, <https://doi.org/10.1016/j.buildenv.2013.09.002>.
 - [19] J. Hang, L. Chen, Y. Lin, R. Buccolieri, B. Lin, The impact of semi-open settings on ventilation in idealized building arrays, *Urban Clim.* 25 (2018) 196–217, <https://doi.org/10.1016/j.ulclim.2018.07.003>.
 - [20] S. Saneinejad, P. Moonen, T. Defraeye, J. Carmeliet, Analysis of convective heat and mass transfer at the vertical walls of a street canyon, *J. Wind Eng. Ind. Aerod.* 99 (4) (2011) 424–433, <https://doi.org/10.1016/j.jweia.2010.12.014>.
 - [21] J. Hang, Z. Luo, X. Wang, L. He, B. Wang, W. Zhu, The influence of street layouts and viaduct settings on daily carbon monoxide exposure and intake fraction in idealized urban canyons, *Environ. Pollut.* 220 (Pt A) (2017) 72–86, <https://doi.org/10.1016/j.envpol.2016.09.024>.
 - [22] A. Di Bernardino, P. Monti, G. Leuzzi, G. Querzoli, Pollutant fluxes in two-dimensional street canyons, *Urban Clim.* 24 (2018) 80–93, <https://doi.org/10.1016/j.ulclim.2018.02.002>.
 - [23] J. Hang, X. Chen, G. Chen, T. Chen, Y. Lin, Z. Luo, X. Zhang, Q. Wang, The influence of aspect ratios and wall heating conditions on flow and passive pollutant exposure in 2D typical street canyons, *Build. Environ.* 168 (2020), 106536, <https://doi.org/10.1016/j.buildenv.2019.106536>.
 - [24] B. Zhang, R. Ooka, H. Kikumoto, Spectral proper orthogonal decomposition analysis of turbulent flow in a two-dimensional street canyon and its role in pollutant removal, *Boundary-Layer Meteorol.* 183 (2022), <https://doi.org/10.1007/s10546-021-00676-4>.
 - [25] Y. Wang, C. Flageul, A. Maison, B. Carissimo, K. Sartelet, Impact of trees on gas concentrations and condensables in a 2-D street canyon using CFD coupled to chemistry modeling, *Environ. Pollut.* 323 (2023), 121210, <https://doi.org/10.1016/j.envpol.2023.121210>.
 - [26] A. Alwi, M.F. Mohamad, N. Ikegaya, A.A. Razak, Effect of protruding eave on the turbulence structures over two-dimensional semi-open street canyon, *Build. Environ.* 228 (2023), <https://doi.org/10.1016/j.buildenv.2022.109921>.
 - [27] J. Liu, S. Cui, G. Chen, Y. Zhang, X. Wang, Q. Wang, P. Gao, J. Hang, The influence of solar natural heating and NOx-O3 photochemistry on flow and reactive pollutant exposure in 2D street canyons, *Sci. Total Environ.* 759 (2021), 143527, <https://doi.org/10.1016/j.scitotenv.2020.143527>.
 - [28] Z. Li, H. Zhang, Y.-H. Juan, C.-Y. Wen, A.-S. Yang, Effects of building setback on thermal comfort and air quality in the street canyon, *Build. Environ.* 208 (2022), <https://doi.org/10.1016/j.buildenv.2021.108627>.
 - [29] H. Yang, T. Chen, Y. Lin, R. Buccolieri, M. Mattsson, M. Zhang, J. Hang, Q. Wang, Integrated impacts of tree planting and street aspect ratios on CO dispersion and personal exposure in full-scale street canyons, *Build. Environ.* 169 (2020), 106529, <https://doi.org/10.1016/j.buildenv.2019.106529>.
 - [30] K. Zhang, G. Chen, X. Wang, S. Liu, C.M. Mak, Y. Fan, J. Hang, Numerical evaluations of urban design technique to reduce vehicular personal intake fraction in deep street canyons, *Sci. Total Environ.* 653 (2019) 968–994, <https://doi.org/10.1016/j.scitotenv.2018.10.333>.
 - [31] J. Hang, Z. Xian, D. Wang, C.M. Mak, B. Wang, Y. Fan, The impacts of viaduct settings and street aspect ratios on personal intake fraction in three-dimensional urban-like geometries, *Build. Environ.* 143 (2018) 138–162, <https://doi.org/10.1016/j.buildenv.2018.07.001>.
 - [32] A. Matzarakis, F. Rutz, H. Mayer, Modelling radiation fluxes in simple and complex environments—application of the RayMan model, *Int. J. Biometeorol.* 51 (4) (2006) 323–334, <https://doi.org/10.1007/s00484-006-0061-8>.
 - [33] Z. Fang, Z. Lin, C.M. Mak, J. Niu, K.-T. Tse, Investigation into sensitivities of factors in outdoor thermal comfort indices, *Build. Environ.* 128 (2018) 129–142, <https://doi.org/10.1016/j.buildenv.2017.11.028>.
 - [34] Z. Li, H. Zhang, C.-Y. Wen, A.-S. Yang, Y.-H. Juan, Effects of frontal area density on outdoor thermal comfort and air quality, *Build. Environ.* 180 (2020), 107028, <https://doi.org/10.1016/j.buildenv.2020.107028>.
 - [35] W. Yang, N.H. Wong, G. Zhang, A comparative analysis of human thermal conditions in outdoor urban spaces in the summer season in Singapore and Changsha, China, *Int. J. Biometeorol.* 57 (6) (2013) 895–907, <https://doi.org/10.1007/s00484-012-0616-9>.
 - [36] M. Allan, G.M. Richardson, H. Jones-Otazo, Probability density functions describing 24-hour inhalation rates for use in human health risk assessments: an update and comparison, *Hum. Ecol. Risk Assess.* 14 (2) (2008) 372–391, <https://doi.org/10.1080/10807030801934796>.
 - [37] C.K. Chau, E.Y. Tu, D.W.T. Chan, J. Burnett, Estimating the total exposure to air pollutants for different population age groups in Hong Kong, *Environ. Int.* 27 (8) (2002) 617–630, [https://doi.org/10.1016/S0160-4120\(01\)00120-9](https://doi.org/10.1016/S0160-4120(01)00120-9).
 - [38] R. Emmanuel, H. Rosenlund, E. Johansson, Urban shading—a design option for the tropics? A study in Colombo, Sri Lanka, *Int. J. Climatol.* 27 (14) (2007) 1995–2004, <https://doi.org/10.1002/joc.1609>.
 - [39] X.-X. Li, C.-H. Liu, D.Y.C. Leung, Numerical investigation of pollutant transport characteristics inside deep urban street canyons, *Atmos. Environ.* 43 (15) (2009) 2410–2418, <https://doi.org/10.1016/j.atmosenv.2009.02.022>.
 - [40] T.R. Oke, Street design and urban canopy layer climate, *Energy Build.* 11 (1) (1988) 103–113, [https://doi.org/10.1016/0378-7788\(88\)90026-6](https://doi.org/10.1016/0378-7788(88)90026-6).
 - [41] X. Xiaomin, H. Zhen, W. Jiasong, The impact of urban street layout on local atmospheric environment, *Build. Environ.* 41 (10) (2006) 1352–1363, <https://doi.org/10.1016/j.buildenv.2005.05.028>.
 - [42] Y. Toparlar, B. Blocken, P. Vos, G.J.F. van Heijst, W.D. Janssen, T. van Hooff, H. Montazeri, H.J.P. Timmermans, CFD simulation and validation of urban microclimate: a case study for Bergpolder Zuid, Rotterdam, *Build. Environ.* 83 (2015) 79–90, <https://doi.org/10.1016/j.buildenv.2014.08.004>.
 - [43] W.H. Snyder, Similarity criteria for the application of fluid models to the study of air pollution meteorology, *Boundary-Layer Meteorol.* 3 (1) (1972) 113–134, <https://doi.org/10.1007/BF00769111>.
 - [44] H. Yang, C.K.C. Lam, Y. Lin, L. Chen, M. Mattsson, M. Sandberg, A. Hayati, L. Claesson, J. Hang, Numerical investigations of Re-independence and influence of wall heating on flow characteristics and ventilation in full-scale 2D street canyons, *Build. Environ.* 189 (2021), 107510, <https://doi.org/10.1016/j.buildenv.2020.107510>.
 - [45] Y. Lin, J. Hang, H. Yang, L. Chen, G. Chen, H. Ling, M. Sandberg, L. Claesson, C.K. C. Lam, Investigation of the Reynolds number independence of cavity flow in 2D street canyons by wind tunnel experiments and numerical simulations, *Build. Environ.* 201 (2021), 107965, <https://doi.org/10.1016/j.buildenv.2021.107965>.
 - [46] S.M. Salim, R. Buccolieri, A. Chan, S. Di Sabatino, Numerical simulation of atmospheric pollutant dispersion in an urban street canyon: comparison between RANS and LES, *J. Wind Eng. Ind. Aerod.* 99 (2–3) (2011) 103–113, <https://doi.org/10.1016/j.jweia.2010.12.002>.
 - [47] C.H. Liu, C.T. Ng, C.C.C. Wong, A theory of ventilation estimate over hypothetical urban areas, *J. Hazard Mater.* 296 (2015) 9–16, <https://doi.org/10.1016/j.jhazmat.2015.04.018>.
 - [48] S. Liu, X. Yang, H. Yang, P. Gao, J. Hang, Q. Wang, Numerical investigation of solar impacts on canyon vortices and its dynamical generation mechanism, *Urban Clim.* 39 (2021), <https://doi.org/10.1016/j.ulclim.2021.100978>.
 - [49] J. Allegri, V. Dorer, J. Carmeliet, Wind tunnel measurements of buoyant flows in street canyons, *Build. Environ.* 59 (2013) 315–326, <https://doi.org/10.1016/j.buildenv.2012.08.029>.
 - [50] A. Walton, A.Y.S. Cheng, Large-eddy simulation of pollution dispersion in an urban street canyon—Part II: idealised canyon simulation, *Atmos. Environ.* 36 (22) (2002) 3615–3627, [https://doi.org/10.1016/S1352-2310\(02\)00260-1](https://doi.org/10.1016/S1352-2310(02)00260-1).
 - [51] Y. Zhang, Z. Gu, C.W. Yu, Impact factors on airflow and pollutant dispersion in urban street canyons and comprehensive simulations: a review, *Curr. Pollut. Rep.* 6 (4) (2020) 425–439, <https://doi.org/10.1007/s04726-020-00166-0>.
 - [52] Z. Li, T. Ming, S. Liu, C. Peng, R. de Richter, W. Li, H. Zhang, C.-Y. Wen, Review on pollutant dispersion in urban areas-part A: effects of mechanical factors and urban morphology, *Build. Environ.* 190 (2021), <https://doi.org/10.1016/j.buildenv.2020.107534>.
 - [53] C.W. Kwon, K.J. Lee, S. Cho, Numerical study of balancing between indoor building energy and outdoor thermal comfort with a flexible building element, *Sustainability* 11 (23) (2019), <https://doi.org/10.3390/su11236654>.
 - [54] G. Chen, X. Yang, H. Yang, J. Hang, Y. Lin, X. Wang, Q. Wang, Y. Liu, The influence of aspect ratios and solar heating on flow and ventilation in 2D street canyons by scaled outdoor experiments, *Build. Environ.* 185 (2020), <https://doi.org/10.1016/j.buildenv.2020.107159>.
 - [55] G. Chen, D. Wang, Q. Wang, Y. Li, X. Wang, J. Hang, P. Gao, C. Ou, K. Wang, Scaled outdoor experimental studies of urban thermal environment in street canyon models with various aspect ratios and thermal storage, *Sci. Total Environ.* 726 (2020), 138147, <https://doi.org/10.1016/j.scitotenv.2020.138147>.
 - [56] J. Hang, G. Chen, Experimental study of urban microclimate on scaled street canyons with various aspect ratios, *Urban Clim.* 46 (2022), <https://doi.org/10.1016/j.ulclim.2022.101299>.